NIR-responsive Photocatalytic Activity (980 nm and 794 nm) of $NaYF_4$:Yb, Tm-TiO_2 and $NaYF_4$:Yb, Tm, Nd@$NaYF_4$:Nd-TiO_2 Colloidal Spheres

WANG YANQI

NATIONAL UNIVERSITY OF SINGAPORE

2014

NIR-responsive Photocatalytic Activity (980 nm and 794 nm) of $NaYF_4$:Yb, Tm-TiO_2 and $NaYF_4$:Yb, Tm, Nd@$NaYF_4$:Nd-TiO_2 Colloidal Spheres

WANG YANQI

(B.Sc., PEKING UNIVERSITY)

A THESIS SUBMITTED

FOR THE DEGREE OF MASTER OF SCIENCE

DEPARTMENT OF CHEMISTRY

NATIONAL UNIVERSITY OF SINGAPORE

2014

Declaration

I hereby declare that this thesis is my original work and it has been written by me in its entirety, under the supervision of LIU XIAOGANG, (in the laboratory S8-05-13), Chemistry Department, National University of Singapore, between Aug. 2013 and July 2014.

I have duly acknowledged all the sources of information which have been used in the thesis.

This thesis has also not been submitted for any degree in any university previously.

Wang Yanqi		
Name	Signature	Date

ACKNOWLEDGEMENT

During the past year in NUS, I have had a lot of memorable experiences and learned many useful knowledge. I would like to thank all the professors, mentors, colleagues and friends who helped and supported me.

Foremost, I want to give my deep and sincere gratitude to my supervisor, Professor Xiaogang Liu, whose wide knowledge, detailed review, and constructive comments have greatly improved and expanded the scope of this thesis. His rigorous scholarship, eruditeness with a keen scientific insight and boundless enthusiasm for scientific work will deeply influence me on my life. I will never forget that he teach us how to practice and improve our English skills on the group meeting.

I would like to give my great thanks to all the members in the Liu's group. Dr. Xiaoji Xie, Dr. Renren Deng, Dr. Xiyan Li, Dr. Yu Wang, Dr. Bo Zhou, Dr. Qianqian Su, Mr. Xiaowang Liu, Mr. Sanyang Han, Mr. Qiang Sun, Mr. Yuhai Zhang, Ms. Xian Qin, Ms. Jing Tian, Mr. Guojun Du, Mr. Xiao Zeng, Ms. Jiahui Xu. Thank you all for your help.

I would like to sincerely acknowledge the financial support of National University of Singapore, and the SPORE program. I would like to thank all the members in the SPORE program.

Table of Contents

SUMMARY

The fundamental researches on photocataiysis have drawn much attention in recent years. The application of photocatalytic materials in solar energy transfer and pollutants degradation provides a very promising method in solving energy crisis and environment pollution. Among all these photocatalysts, titanium dioxide have been widely studied and applied in practice due to its physical stability, low cost, and high photocatalysis efficiency. However, the solar energy utilization efficiency of typical TiO_2 materials is constrained by its high possibility of electron-hole recombination and large band gap. In order to enhance the photocatalytic efficiency and solar energy utilization rate of TiO_2, modification of titanium dioxide have been a hot research topic.

This study fabricated two new kinds of photocatalyst (NaYF4: Yb, Tm-TiO_2 and $NaYF_4$:Yb/Tm/Nd@$NaYF_4$:Nd-TiO_2 colloidal spheres) successfully for NIR-responsive photocatalysis. The optimal synthesis conditions and doping concentration of rare earth ions for the new materials are established. TEM and XRD analysis confirm this 3D colloidal spheres structure. UV light energy emitted from upconversion materials has been utilized by this material to generate photo-generated electron-hole pairs, which

then combine with the surface water or hydroxyl to generate sufficient amount of •OH for photocatalytic degradation of organic pollutants. These new materials present very good photocatalytic activity and could enhance utilization efficiency for solar energy. $NaYF_4$:Yb/Tm/Nd@$NaYF_4$:Nd-TiO_2 colloidal spheres can not only utilize 794 nm light but also 980 nm light when irradiated by solar light. More importantly, this new material can avoid energy consumption by water and consequent heating effect under 980 nm excitation. More than 85% MB can be degraded by these two materials (25 ^{o}C, 4 h, 2 g/L photocalysts), which confirms them good potential for photcatalytic application.

LIST OF FIGURES

LIST OF ABBREVIATION AND SYMBOLS

CW	continuous wave
EMU	energy migration-mediated upconversion
ETU	energy transfer upconversion
ESA	excited-state absorption
PA	photon avalanche
SDS	sodium dodecyl sulfate
SPECT	single-photon emission computed tomography
TEM	transmission electron microscope
XRD	X-ray diffraction
MB	Methylene Blue

CHAPTER 1: Introduction

Since the formation of human civilization, the development of human society is accompanied by acquirement and utilization of natural resources. The current global economy relied on energy provided by oil, coal, and natural gas as well as resources extracted from minerals. Predatory consumption of traditional non-renewable resources caused energy crisis of human society accompanied with destruction and pollution of the natural environment. In the twenty-first century, "energy crisis" and "environment pollution" have become the two critical constraints to sustainable development of human society. Photocatalysis through solar light can be a very promising method in solving these two problems [2].

1.1 Introduction of Nanomaterials

Nanomaterials have drawn much attention since their first studies in 1970s~1980s. Generally, the size of nanomaterials is between the range of 1 ~ 100 nm in at least one dimension. With this nanoscale range between microscopic and macroscopic, nanomaterials show specific surface and interface effects, small size effect, quantum size effect and macroscopic quantum tunneling effect, which make them exhibit excellent mechanical, thermal, optical and electrical properties. Therefore, nanomaterials have broad

applications in materials, medicine, biotechnology and environmental protection. Moreover, nanoparticles now have been incorporated in our daily life. More than one thousand nanoparticle-related products are now commercially available, including health care products, electronic products, and food products and so on [3].

Based on the spatial dimension, nanomaterials can be divided into zero -dimensional clusters and nanoparticles, one-dimensional multi-layer films and nanotubes (nanorods, nanowires), two-dimensional and three-dimensional nanofilms and assembly material. Zero-dimensional nanomaterials include TiO_2 nanoparticles, gold nanoparticles, upconversion nanoparticles, silica nanoparticles and so on.

Among various nanoparticles, upconversion nanoparticles is one kind of widely studied nanomaterials, due to their applications in optical, biosensing, bioimaging, and barcoding. The term upconversion describes an anti-Stokes emission of higher energy photon which is excited by the two or more lower energy pump photons [4].Typically, the upconversion nanoparticles are lanthanide-doped nanoparticles, which comprise an insulating host matrix and lanthanide dopant ions embedded in the host lattice. Due to the unique intra-configurational $4f^n$ electron transitions within the dopant lanthanide ions, these upconversion nanoparticles show advances, such as high photostability,

large anti-Stokes shift and sharp emission bandwidths, over other luminescent materials [5]. Upconversion nanomaterials could convert near infrared light to ultra-violet and visible light, which is likely to be useful in solar energy utilization.

Apart from upconversion nanomaterials, semiconductor materials are also very useful nanomaterials. Due to their unique quantum size effect, semiconductor materials exhibit wide energy gap between conduction band and valence band thus strong redox ability. Nano-TiO_2 has been widely studied in photocatalysis applications owing to its low cost, high efficiency, non-toxicity, biocompatible, and environment stability since 1972 [6].

1.2 Optical Property of Upconversion Nanoparticles

One of the most interesting and remarkable properties of upconversion nanoparticles is the upconversion phenomenon, which is mainly due to the lanthanide dopants. Typically, there is sequential absorption of two or more photons by the metastable, long-lived energy states of the lanthanide ions in the upconversion process. Therefore, the lanthanide ions are populated to higher excited state from which the upconversion emission occurs [4].The upconversion effect is used in infrared quantum counting detectors, solid-state lasers, temperature sensors, light and display devices as well as other areas of

biomedical imaging [5, 7].

Most of the current upconversion effect is based on trivalent rare earth ion transitions between the 4f electrons. The luminous efficiency of rare earth ions is more stable because 4f electron transitions are less influenced by the matrix. Typically, Er^{3+}, Tm^{3+} and Ho^{3+} are used as upconversion luminescence agent because they all have terraced energy levels, which could absorb light energy and transfer energy to the next energy level. Yb^{3+} is often used as sensitizer to enhance upconversion efficiency and incorporated into the matrix lattice with activators.$^2F_{5/2} \rightarrow {}^2F_{7/2}$ transition of Yb^{3+} ensured its strong absorption between 900-1100 nm. Yb^{3+}-Er^{3+} and Yb^{3+}-Tm^{3+} are the most widely studied doping ion pairs [8] (Fig. 1.1). Furthermore, upconversion based on 800 nm excitation with Nd^{3+} as a sensitizer has also been reported [9].

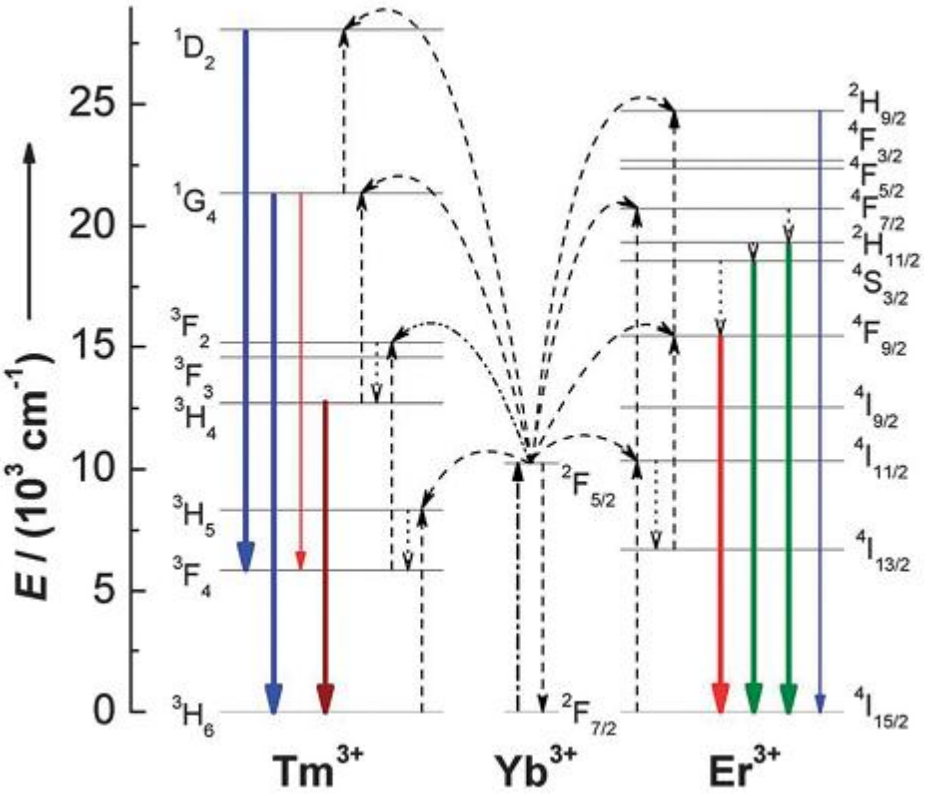

Figure 1.1 Proposed upconversion mechanisms for Yb^{3+}-Tm^{3+} and Yb^{3+}-Er^{3+} couples under 980 nm diode laser excitation. The dash-dotted, dashed ,dotted, and full arrows represent photon excitaiton, energy transfer, multiphonon relaxation, and emission processes, respectively.

Figure 1.2 presents several types of upconversion process. The most common four upconversion processes are excited-state absorption (ESA), energy transfer upconversion (ETU), photon avalanche (PA) and energy migration-mediated upconversion (EMU). Among all the types, the ETU process is the most efficient upconversion process and most of the upconversion nanoparticles used today take advantage of this mechanism [10]. ESA is the basic process of upconversion with only one ion participating. It is

the process that an ion from the ground state is excited to a higher excited state through continuous multi-photon absorption. As shown in Fig. 1.2 (e), the electron at the ground state transits to the metastable state after absorbing a photon, and further transits to a high-energy state after absorbs another photon. When it returns to the ground state, it can emit a high-energy photon. In the ETU process, one photon will be absorbed by one ion firstly and then a subsequent nonradiative energy transfer from neighboring ions would result in the population of a highly excited state of the emitting ion. So the dopant concentration that determines the average distance between the neighboring dopant ions has a strong influence on the upconversion efficiency of an ETU process [5]. Photon Avalanche (PA) is a combination of the first two. After absorbing energy, the electron in the metastable state is excited to a higher energy state and there is cross-relaxation between the ground state energy level and the higher energy level. Ions are accumulated on the metastable state like the avalanche. This process depends on the number of metastable particles. When the doping concentration is sufficiently high and exceeds the threshold of pump power, this phenomenon occurs. Typically, Y^{3+} is used as the host material due to its inert property and Yb^{3+} is used as a sensitizer to transfer energy to neighboring emitting ions because it has only one excited state on 4f orbit; while Er^{3+}, Tm^{3+} and Ho^{3+} are the most commonly used emitting ions.

Energy migration-mediated upconversion (EMU) process was proposed by our group recently, involving the utilization of four types of lanthanide ions doped in different region of a core-shell structure [1]. In the EMU process, the gadolinium ions exist both in the core and the shell lattice and it can generate sublattice-mediated energy migration effect, which enables a wide range of upconversion emissions in different types of lanthanide activators without long-lived intermediary energy states. This new mechanism could be useful in the color tuning of upconversion nanoparticles. Notably, the emission of upconversion nanoparticles could be finely tuned by the host materials and dopant concentrations utilizing either ETU process or EMU process [11].

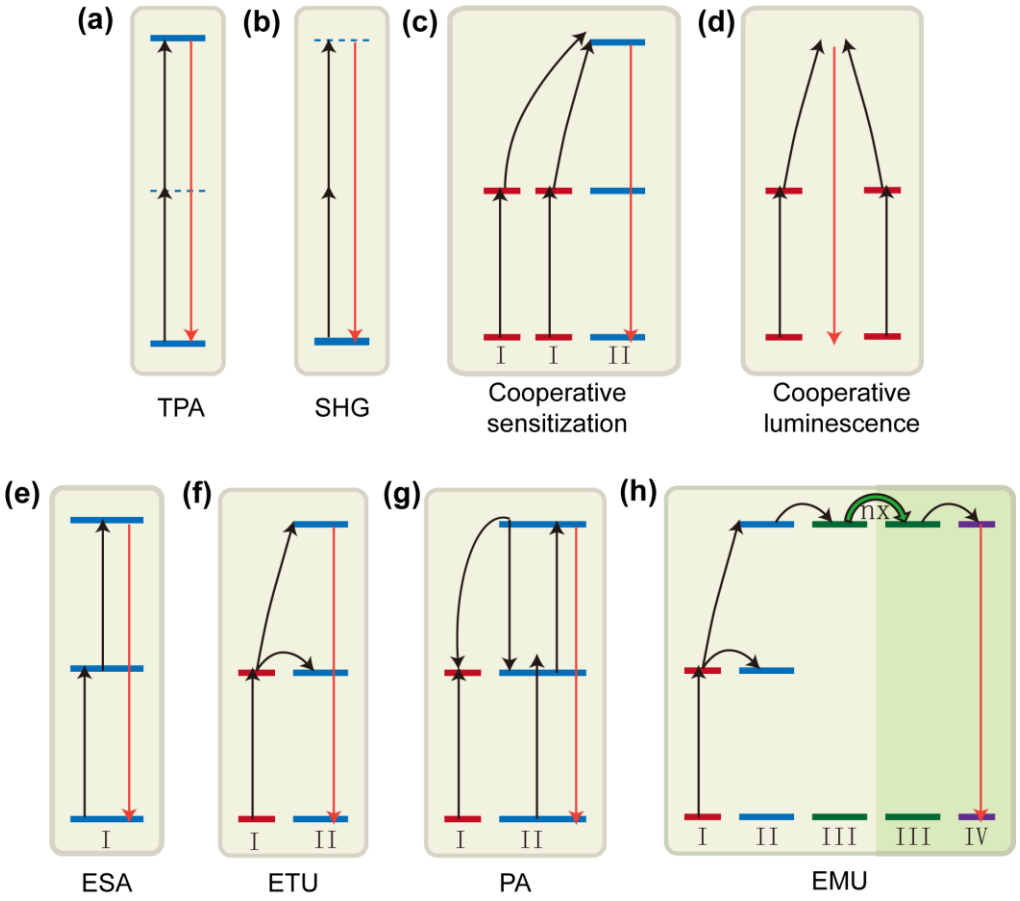

Figure 1.2 Typical upconversion processes. (a) 2-photon absorption (TPA). (b) Second-harmonic generation (SHG). (c) Cooperative sensitization. (d) Cooperative luminescence. (e) Excited state absorption (ESA). (f) Energy transfer upconversion. (g) Photon avalanche (PA). (h) Energy migration-mediated upconversion (EMU). (Reprinted with permission. [1] Copyright 2013, Nature Publishing group.)

Because almost half of solar light consists of NIR light but most of semiconductor materials can only make use of UV or visible light, so it will be meaningful to convert NIR light of solar to UV or visible light. There are a lot of research studying the integration of upconversion materials and semiconductors for solar cells, photocatalysis, and photocatalytic water

splitting [12]. Typically, Er^{3+} is used as activator in combination with solar cells because it can emit visible light and Tm^{3+} is used as activator in combination with photocatalysis because it can emit UV light.

1.3 Photocatalysis of Titanium Dioxide

As early as a century ago, photocatalytic phenomenon generated by coating of TiO_2 had been reported. In 1972, Japanese scientists A. Fujishima and K. Honda split water into hydrogen and oxygen in the TiO_2 electrode and illustrated the relevant mechanism of photocatalytic and photoelectrocatalysis for the first time. This landmark discovery brought the photocatalytic technology into the historical stage. Through photocatalytic technology, the clean and sustainable solar energy can be utilized at room temperature. These photocatalytic technology (such as production of hydrogen by water photolysis, photocatalytic degradation of water and air pollutants, photocatalytic self-cleaning surfaces) can provide clean energy for human at the same time effectively reduce environmental pollution, ensure sustainable development of human society. In recent years, photocatalytic technology has been widely applied in energy, military, environmental protection, medical, construction, automotive industry, clothing, etc., resulting in a lot of social and economic benefits. It has become the focus of current science research and

industrial application.

Energy band structure of the semiconductor material is not continuous. Electrons can move freely in the valence band (VB) and the conduction band (CB); however electron can't reach the area between the top of the valence band and he bottom of conduction band, which is called the forbidden band (Band Gap). The band gap of TiO_2 is approximately 3.2 eV. The electron in the valence band could be excited to the conduction band and a corresponding hole will generate in the valence band when the semiconductor absorb a photon whose energy exceeds band gap energy.

The principle of photocatalytic reaction is that the photocatalyst can generate holes (h+) and electron (e-) which can degrade pollutants under light irradiation. The most studied photocatalysts are semiconductor metal oxides and sulfides, such as TiO_2, ZnO, CdS, WO_3 and SnO_2 and the like. When light energy is equal to or larger than the energy band gap of semiconductors, the electrons in valence band are excited into the conduction band across the band gap and create a corresponding hole at the same time. The photogenerated holes and electrons will separate and migrate to different positions of semiconductor particle surfaces. These holes and electrons have strong redox ability, which can facilitate oxidation-reduction reaction with the matter adsorbed to the particle surface. Meanwhile, it is also possible for the

recombination of the photogenerated holes and electrons. If there is no proper capture agent, the photogenerated holes and electrons will be consumed through recombination in a few microseconds; if there is a proper capture agent capturing holes and electrons, the recombination will be inhibited and the redox reaction occurs [13].

Titanium dioxide is one of the most common photocatalyst. It has a lot of good property, such as high oxidation efficiency, no toxicity, high light stability, high chemical inertness, and environmentally friendly. The photocatalytic reaction mechanism of TiO_2 is illustrated in Fig. 1-1. In TiO_2 aqueous suspension systems, H_2O, OH^- and organics can be capture agent. These matters could generate hydroxyl radical (•OH) oxidative after the capture of the holes. •OH is the strongest oxidant in the water and has almost no selectivity for substrates. The capture agent of photo-generated electron is mainly O_2 adsorbed on TiO_2 surface. O_2 can produce • OH after capturing electrons. Meanwhile, the photo-generated electron also has strong reduction ability.

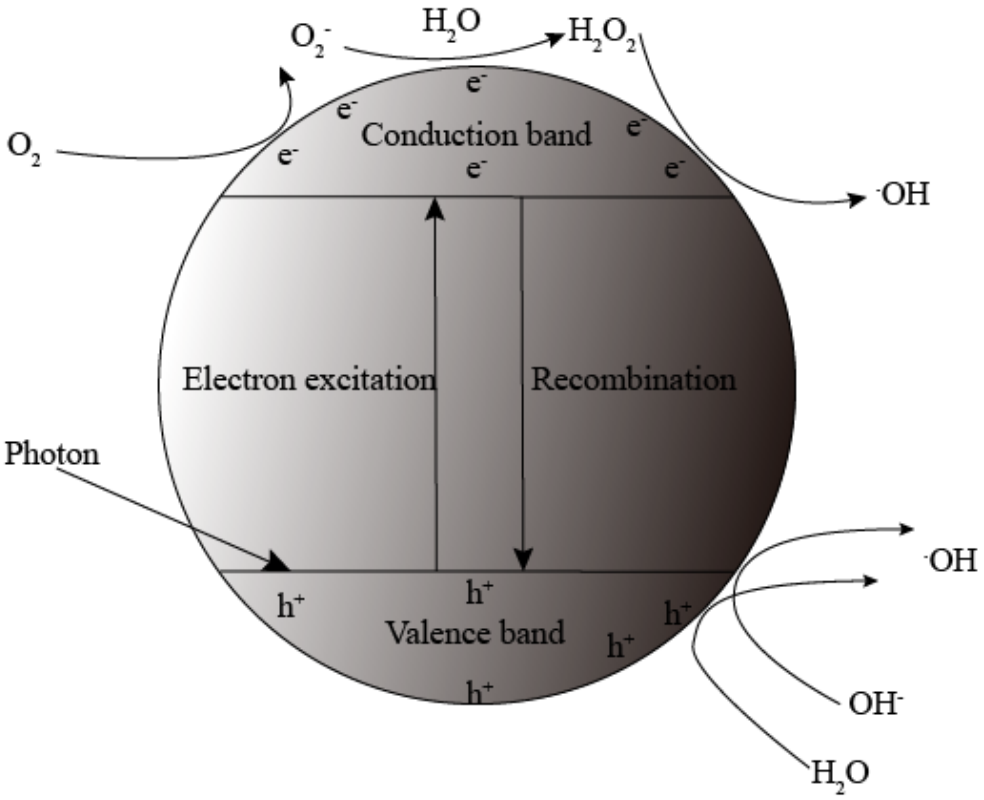

Figure 1.3 TiO_2 photocatalysis mechanism

The basic reaction formulas of photocatalytic principle are as follows:

$$TiO_2 + h\nu \rightarrow TiO_2 + h^+ + e^-$$

$$h^+ + e^- \rightarrow \text{heat}$$

$$H_2O \rightarrow H^+ + OH^-$$

$$h^+ + OH^- \rightarrow \cdot OH$$

$$h^+ + H_2O \rightarrow \cdot OH + H^+$$

$$e^- + O_2 \rightarrow \cdot O_2^-$$

$$O_2^- + H^+ \rightarrow HO_2\cdot$$

$$2\ HO_2\cdot \rightarrow O_2 + H_2O_2$$

$$H_2O_2 + \cdot O_2^- \rightarrow \cdot OH + OH^- + O_2$$

$$H_2O_2 + h\nu \rightarrow 2\cdot OH$$

$$e^- + \bullet OOH + H_2O \rightarrow H_2O_2 + OH^-$$

$$e^- + H_2O_2 \rightarrow \bullet OH + OH^-$$

$$h^+ + \bullet O_2^- \rightarrow {}^1O_2$$

$$\text{Organics} + (\bullet OH, \bullet O_2^-, \bullet OOH, {}^1O_2, \text{etc}) \rightarrow CO_2 + H_2O + \ldots$$

In the past two decades, TiO_2-based photocatalytic materials played an important role in the degradation of pollutants in water bodies. Compared to conventional wastewater treatment, photocatalytic treatment has unique advantages: first, the cost is relatively inexpensive because it only needs water, oxygen, sunlight and consumes almost no other artificial additives and energy consumption; secondly, the photocatalytic reaction can be carried out at atmospheric pressure and room temperature, which requires no strict operation and device conditions; thirdly, it can degrade a large number of water pollutants, including oil and grease, aromatic compounds, polymer, dyes, surfactants, herbicides and pesticides and most of the degradation products are CO_2 and H_2O, which reduces the secondary pollution.

However, the band gap of titanium dioxide is approximately 3.2 eV, which can only be excited by UV light shorter than 380 nm. Therefore, the utilization

rate of traditional TiO_2 for practical use is too low. How to improve the NIR and visible light absorption rate of TiO_2 will be a meaningful research project. Typically, there are two ways to enhance solar energy utilization efficiency of TiO_2, one is doping with other elements to decrease the bandgap of TiO_2 (Figure 1.4 and 1.5) and the other is convert NIR light to UV light to be utilized.

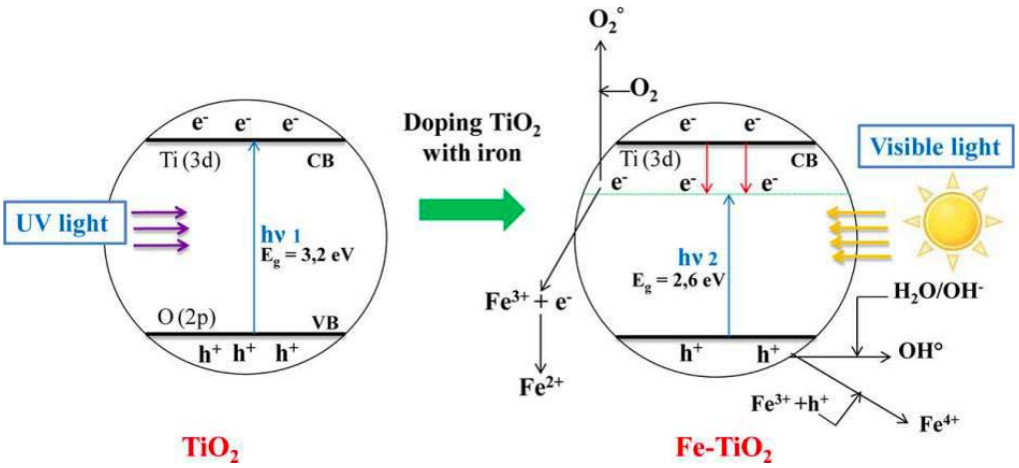

Figure 1.4 Schematic energy level of iron doping TiO_2 (Reprinted with permission from [14] Copyright 2013, American Chemical Society.)

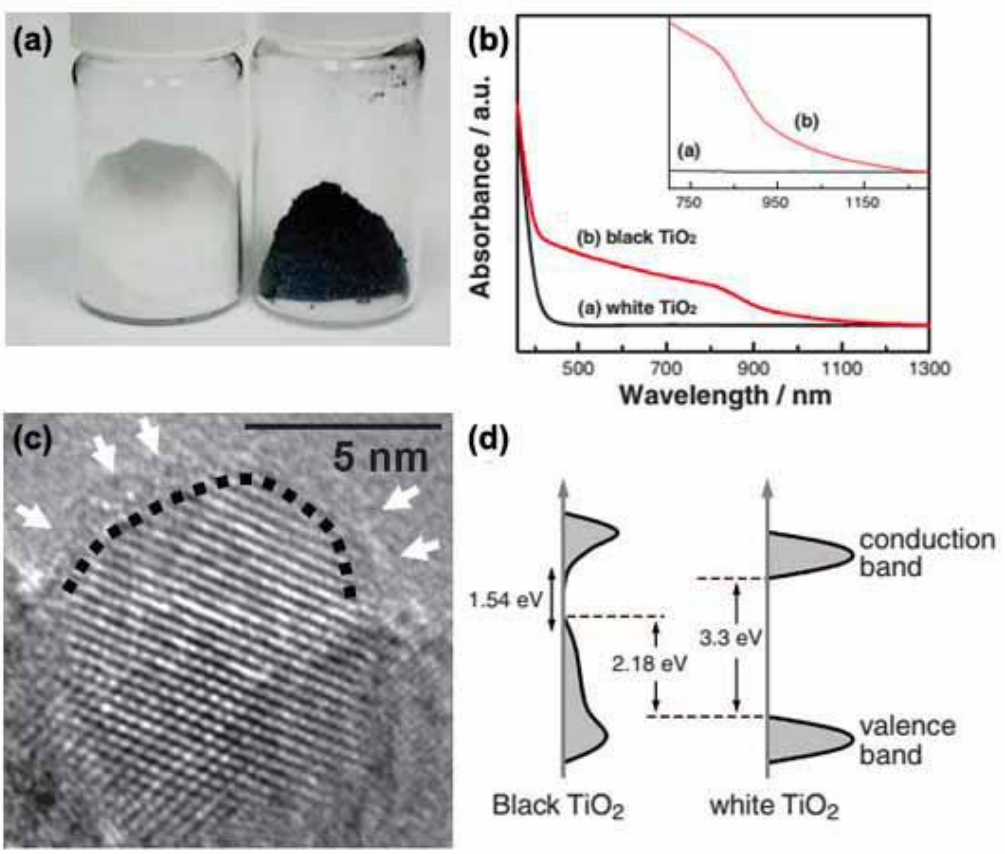

Fig. 1.5 (a) A photo comparing TiO_2 (left) and H-doped TiO_2 (right); (b) Spectral absorbance of TiO_2 and H-doped TiO_2; (c) HRTEM images of H-doped TiO_2 nanocrystals and (d) Schematic illustration of the DOS of H-doped TiO_2, as compared to that of unmodified TiO_2 (From [15]. Reprinted with permission from AAAS).

1.4 The Integration of Upconversion Materials and Titanium Dioxide

There are two ways to use upconversion materials to assist photocatalytic materials: rare earth ions doped photocatalytic materials and upconversion materials/photocatalytic materials heterostructure composite. The former one doped rare earth ions directly into photocatalyst. Yan et al.[16] reported that uniformly doping of Yb^{3+} and Tm^{3+} in porous TiO_2 can effectively enhance the

absorption of photocatalyst in NIR region and improve its photocatalytic degradation efficiency of Rhodamine B dye. Unfortunately, the disadvantage of these materials is obvious: TiO_2 is not a good luminous matrix and the incorporation of trivalent rare earth ions will inevitably provide new places for the recombination of the photo-generated electron-hole pairs. Therefore, relatively little research studied such doped photocatalysts. On the other hand, there are a lot of studies about upconversion materials/photocatalysts heterostructure composite. In such a composite structure, energy will be transferred to upconversion materials component in the form of longer wavelength excitation light, and then transferred to photocatalysts component in the form of shorter wavelength light [17]. For example, Qin et al. [17] coated anatase titanium dioxide in the outer surface of YF_3: Yb^{3+}, Tm^{3+}, which can degrade methyl orange and methylene blue in the NIR light irradiation.

Many studies assembled upconversion materials and titanium dioxide to core-shell structure for photocatalysis under NIR light [18].However, the surface area of these core-shell structure is small, which is not helpful for its adsorption capacity thus the photocatalytic rate [19]. Moreover, the shell thickness of core-shell structure needs precise control since less UV light will be utilized if the shell is too thin, and if the shell is too thick, a lot of the incident NIR light will be attenuated, meanwhile the surface TiO_2 will be less

activated due to the weakened UV light arriving at the external surface [20].

1.5 Objectives

In view of the above review, the core-shell structure of $NaYF_4$: Yb^{3+}, Tm^{3+} have been explored for photocatalysis under NIR light. However, it is worthwhile to point out that there are still many challenges, which include the limited surface area and the difficulty in controlling the shell thichness. The objectives of this study are summarized below.

Assemble a new 3D colloidal sphere structure of $NaYF_4$: Yb^{3+}, Tm^{3+}-TiO_2 hybrid and $NaYF_4$: Yb, Tm, Nd@$NaYF_4$: Nd-TiO_2 hybrid.

Enhance the active surface area and thus the photocatalytic efficiency through this 3D colloidal sphere design.

Extend the excitation source of the NIR responsive photocatalysis.

The results of this present study may have significant impact on the photocatalysis of organic pollutant under different NIR light excitation. The newly designed structure could make fully use of the total surface area of $NaYF_4$: Yb^{3+}, Tm^{3+} and TiO_2 nanoparticles. Moreover, the NIR responsive photocatalysis under 794 nm excitation could offer a new direction for the utilization of solar light with different wavelength.

CHAPTER 2: NIR-responsive Photocatalytic Activity (980 nm) of $NaYF_4$: Yb, Tm-TiO_2 Colloidal Spheres

2.1 Introduction

The application of photocatalysis for pollution treatment has attracted a great deal of attention in recent years. Titanium dioxide, as one of the most investigated semiconductor photocatalysts, has been widely studied due to its low cost, high efficiency, non-toxicity, biocompatible, and environment stability. Unfortunately, this photocatalyst requires UV light to be activated because of its large bandgap of ~3.2 eV. As we all know, UV light only occupies ca. 5% of the solar energy (Fig.2.1). The visible light and near-infrared light, which possess ca. 40% and ca. 55%, respectively of the solar energy, can't be utilized by titanium dioxide. Therefore, the utilization rate of solar energy by titanium dioxide is no more than 5%. So making sufficient use of the photons with lower energy than the bandgap energy is very important for the large-scale application of titanium dioxide to solve energy crisis and environmental pollution in the future.

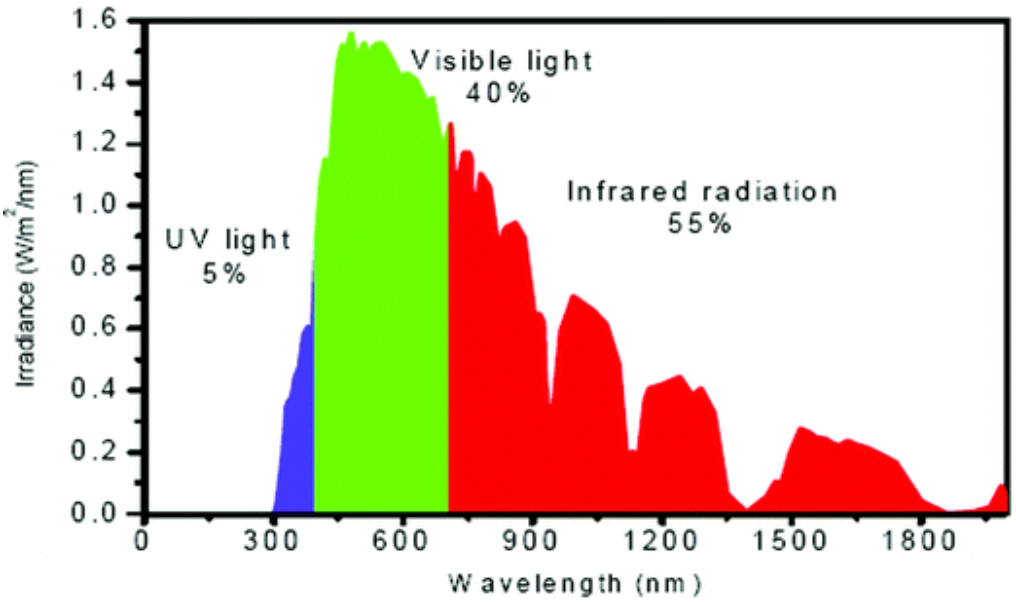

Figure 2.1 Solar energy distribution

In recent years, much effort has been devoted to enhance the solar light utilization efficiency of titanium dioxide by extending its absorption region to the visible light and even NIR light. To reach this goal, several strategies have been proposed, such as anionic and cationic doping, noble metals deposition, grapheme/carbon nanotubes modification, and coupling with other semiconductors [21]. However, the overall catalytic capability was found to decrease because the introduced materials may increase the photogenerated electron-hole pair recombination in certain degree [22].

The development of nanotechnology opens a new way to obtain nanomaterials with novel and desirable properties. In recent years, rare earth doped material has become one of the most efficient fluorescent material

because of its narrow emission bandwidth, long fluorescence lifetime, low biological toxicity and high physical and chemical stability. Compared to the traditional organic fluorescent dyes, rare earth doped material's stability is higher and their preparation process is simpler; compared to the relatively popular quantum dot fluorescent material, toxicity of rare earth doped material is smaller, and luminous character of that is more stable. More importantly, the upconversion materials could be synthesized when using suitable rare earth ion doping. These upconversion materials can transform near-infrared light into ultraviolet and visible light and they have been applied in biological imaging mark, solar energy conversion, photodynamic therapy, and other fields.

The upconversion materials have been discovered and studied for emission of visible and UV light under NIR light excitation. It is reasonable that titanium dioxide can absorb UV light emitted from upconversion materials for efficient photocatalysis reactions. There are two typical ways to combine upconversion materials and titanium dioxide: direct composite and core-shell structure. The former one mixed the two materials under certain condition and linked these two together through intermolecular forces. Ren et al. reported a composite composed of P25, YF_3: Yb^{3+}, Tm^{3+}, and graphene for waste water purification [23]. Li et al. reported that uniformly doping of Yb^{3+}

and Tm^{3+} in porous TiO_2 can effectively enhance the absorption of photocatalyst in NIR region and improve its photocatalytic degradation efficiency of Rhodamine B dye [16]. Xu et al. prepared N-TiO_2/$NaYF_4$: Yb^{3+}, Tm^{3+} nanocomposite for near-infrared-triggered drug release [24]. However, the direct composite of upconversion materials and titanium dioxide shows apparent shortcomings: First, the liquid environment will lead to serious surface quenching and reduced luminous efficiency [25]; second, because of always being covered by luminescent material, photocatalyst can't be in sufficient contact with water, oxygen, and substrate; third, the separation of these two materials due to weak binding between them will lead to reduction of energy transfer efficiency.

Therefore, in recent years, more and more researchers studied the core-shell heterostructure. Upconversion materials are wrapped by titanium dioxide in the core, which can suppress surface quenching; photocatalytic materials act as the shell so that it can not only fully react with surroundings, but also protect the upconversion materials. The full contact between these two materials play an important role in energy transfer. Li et al. coated CdS nanocrystals on the outer surface of $NaYF_4$: Yb, Tm micron rod, and used the assembled materials to degrade organic dyes [26]. Li et al. coated nano-porous TiO_2 onto YF_3 to improve the absorption of near infrared light and catalytic

activity as well as increase the surface area [27]. Huang et al. doped Yb and Er ions into CaF_2@TiO_2 core-shell materials and improved photocatalytic activity through moderating ion doping concentration [28].Qin et al. coated anatase titanium dioxide in the outer surface of YF_3: Yb^{3+}, Tm^{3+}, which can degrade methyl orange and methylene blue in the NIR light irradiation [17]. Tang et al. prepared $NaYF_4$: Yb^{3+}, Tm^{3+}@TiO_2 nanoparticles for methyl blue degradation [18b].

Although a lot of such core-shell heterostructures composite photocatalyst has been reported, there are still some problems to be solved: First, on one hand, it is difficult for synthesis of core-shell heterostructures based on TiO_2 shell due to its spontaneous nucleation and aggregation, which will affect the coating process. On the other hand, it is easier for these titanium precursor (alkoxide) becoming into amorphous TiO_2, which has much lower catalytic activity than crystallization TiO_2. In order to improve the crystallinity, it is necessary to conduct heat treatment at high temperature [17], which will result in agglomeration, decreased dispersibility, possible damage of core-shell structure. Second, the thickness of TiO_2 shell is always ignored. If the shell is too thick, it will affect the performance of luminescent material inside, and if too thin, it can't protect the core materials and make full use of the light emitted from the core. Therefore, it is important to regulate the thickness of

TiO_2 shell, which is a very difficult task [20]. Third, the interface surface between the core and the shell is helpless for adsorption and photocatalysis because it can't be in contact with surroundings. Therefore, a new 3D colloidal sphere structure of upconversion materials and titanium dioxide that can avoid the above problems was assembled in this chapter.

2.2 Synthesis and Characterization

2.2.1 Materials

Ammonium bicarbonate (NH_4HCO_3, 99.9%), triethylamine ($(C_2H_5)_3N$, >99%), titanium butoxide ($Ti(OCH_2CH_2CH_2CH_3)_4$, 97%), yttrium(III) acetate hydrate ($Y(CH_3CO_2)_3 \cdot xH_2O$, 99.9%), ytterbium(III) acetate hydrate($Yb(CH_3CO_2)_3 \cdot 4H_2O$, 99.9%), thulium acetate hydrate ($Tm(CH_3CO_2)_3 \cdot$ xH2O, 99.9%), sodium hydroxide (NaOH, >98%), ammonium fluoride (NH_4F,>98%), 1-octadecene (90%), oleic acid (90%), cyclohexane (>99%), sodium dodecyl sulfate (SDS, >99%), methylene blue (MB, Fig. 2.2) were all purchased from Sigma-Aldrich and used as received unless otherwise noted. All other chemicals were purchased from Sigma-Aldrich unless otherwise noted.

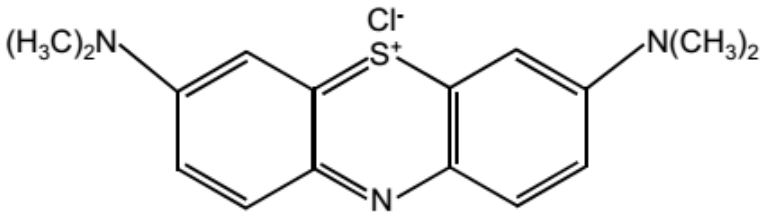

Figure 2.2 Molecular formula of methylene blue.

2.2.2 Characterization

Low-resolution transmission electron microscopy (TEM) measurements were carried out on a JEOL-1400 transmission electron microscope (JEOL) operating at an acceleration voltage of 100 kV and high-resolution TEM measurements were carried out on a JEOL-JEM 2010F field emission transmission electron microscope operated at an acceleration voltage of 200 kV. Powder X-ray diffraction (XRD) data was recorded on a Siemens D5005 X-ray diffractometer with Cu Kα radiation (λ=1.5406 Å). The photoluminescence measurements were measured using a Spectra Physics Ti: sapphire oscillator (Tsunami) as the excitation source for ~800 nm excitation. UV-vis transmission spectrum was recorded on a SHIMADZU UV-3600 spectrophotometer. The CW laser beam was focused onto samples contained in a cuvette with path length of 1 cm. The emission from the samples was collected at an angle of 90^{o} to the excitation beam by a pair of lenses and an optical fiber that was connected to a monochromator (Acton, Spectra Pro

2300i) coupled CCD (Princeton Instruments, Pixis 100B). A short pass filter with a cutoff wavelength of 750 nm was placed before the monochromator to minimize scattering from the excitation beam. The upconversion luminescence spectra under 980 nm excitation were recorded in an Edinburgh FSP920 equipped with a photomultiplier (PMT), in conjunction with 980 nm diode laser (100 mW). The near-infrared photoluminescence spectrum was excited by monochromatic light from a standard Xe lamp (450 W) passed through a monochromator (FSP920, Edinburgh).

2.2.3 Synthesis of $NaYF_4$: Yb^{3+}, Tm^{3+} Nanoparticles

In a typical experiment [1], 2 mL water solution of $Ln(CH_3CO_2)_3$ (Ln = Y, Yb, 0.2 M, Ln = Tm, 0.02 M) was added to a 50-mL flask containing 3 mL of oleic acid. The mixture was heated at 150 ^oC for 30 min to remove water from the solution. Then 7 mL of 1-octadecene was quickly added to the flask and the resulting mixture was heated at 150 ^oC for another 30 min before cooling down to 50 ^oC. Shortly thereafter, 6 mL of methanol solution containing NH_4F (4 mL, 1.6 mmol) and NaOH (2 mL, 1 mmol) was added and the resultant solution was stirred for 30 min. The system temperature was heated to 100 ^oC to evaporated methanol and then argon was used to replace the air in this system. The solution was heated to 290 ^oC under argon for 1.5 h and then

cooled down to room temperature. The resulting nanoparticles with a yield of 80 mg were precipitated by addition of ethanol, collected by centrifugation at 6000 rpm for 5 min, washed with ethanol several times, and re-dispersed in 4 mL of cyclohexane.

2.2.4 Synthesis of Titanium Dioxide Nanoparticles

In the typical synthesis procedure of TiO_2 nanoparticles [29], 0.5 g NH_4HCO_3, 7 mL OA, and 3 mL triethylamine were mixed at room temperature by magnetic stirring. Then $Ti(OBu)_4$ (1 mL) was added dropwise into the solution. After continued stirring at room temperature for 5 min, the solution was transferred into a Teflon-lined, stainless autoclave at 150 ^oC for 24 h. TiO_2 nanoparticles were obtained.

2.2.5 Synthesis of $NaYF_4$: Yb^{3+}, Tm^{3+}-TiO_2 Hybrid

In a general preparation of water-dispersed 3D colloidal spheres from oil-dispersed NCs [30], SDS (200 mg) was added to deionized water (20 mL). A solution containing upconversion materials (0.5 mL) and TiO_2 (1.5 mL) in cyclohexane was added to the aqueous solution. This system was then emulsified by ultrasonic treatment together with magnetic stirring. The cyclohexane was removed by heating at 70 ^oC with constant stirring for 4 h to

assemble the NCs into 3D spheres. After the reaction was cooled to room temperature, the products were collected and purified by repeated centrifugation and were redispersed. The final products were stored in water. The procedures for bottom-up self-assemblies of single nanocrystals were similar to this one, except that the NC type, or NC concentration was altered.

2.3 Experimental Design

2.3.1 Photocatalytic Experiments

Photocatalysis was performed via monitoring methylene blue (MB) degradation by measuring the optical absorption using a Shimadzu UV-3600 spectrophotometer. In a typical experiment, 4 mg of the $NaYF_4$: Yb^{3+}, Tm^{3+}-TiO_2 hybrid was dispersed into a quartz cuvette containing 2 mL of MB aqueous solution (15 mg L^{-1}) and then kept in the dark prior to irradiation for reaching adsorption−desorption equilibrium of MB on the surface of materials beforee irradiation. A laser of 980 nm with a power of 2 W was used as the irradiation source. After irradiation of 980 nm light for a designated time, 0.3 mL of the MB aqueous solution was taken out and centrifuged for UV−vis absorbance measurements. The concentration of MB solution at each time interval was calculated using the calibration curve of the characteristic absorption peak of MB (663 nm) of the standard solution. The schematic

diagram of the equipment for photocatalytic experiments is shown in Figure 2.3.

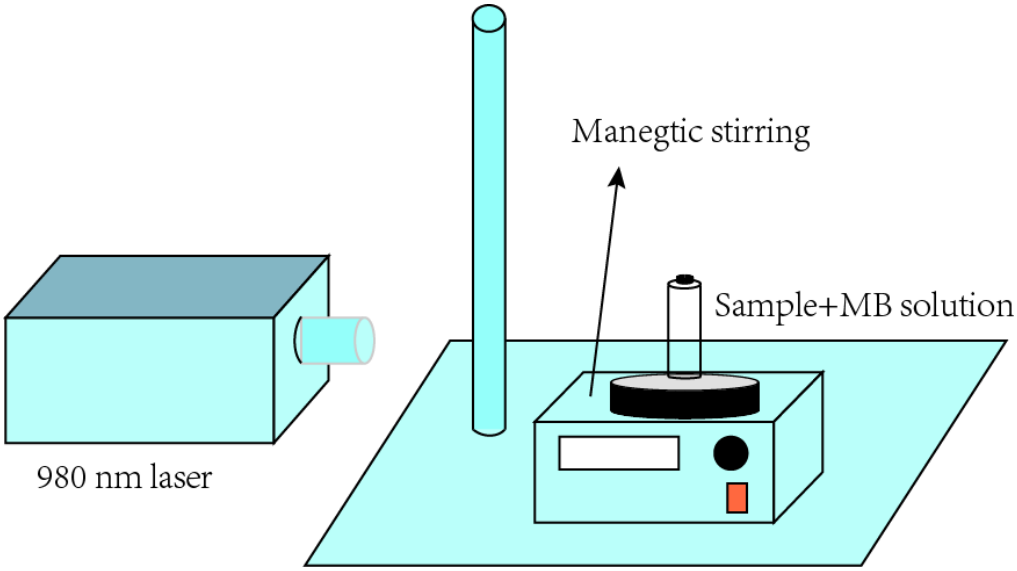

Figure 2.3 schematic diagram of the equipment for photocatalytic experiments

2.3.2 Detection of Photogenerated OH Radicals

The generation of radicals in solution was detected by the photoluminescence measurement with terephthalic acid as a probe molecule. 2-Hydroxyterephthalic acid, a highly fluorescent compound, could be formed when the produced •OH interacted with the terephthalic acid in the water solution [18]. The procedure was similar to that of the photocatalytic activity test except that the dye aqueous solution was replaced by the terephthalic acid and NaOH mixture aqueous solution. Terephthalic acid (3×10^{-3} M)was dissolved in NaOH (1×10^{-2} M)solution. In a typical process, 3 mg of $NaYF_4$: Yb^{3+}, Tm^{3+}-TiO_2 hybrid was mixed with 3 mL of terephthalic acid solution, then the

mixture was irradiated with a 980 nm NIR laser. Every 30 min, 0.6 mL of the suspensions were collected and then centrifuged. After that, photoluminescence (PL) measurement was used to monitor the hydroxyl terephthalate anion with an excitation wavelength of 320 nm.

2.4 Results and Discussion

2.4.1 The Optimal Synthesis Conditions

$NaYF_4$ was the most studied upconversion luminescence fluoride host and it was chosen in this study due to the high efficiency of upconversion transition in the $NaYF_4$ host system. In order to obtain the upconversion auxiliary photocatalyst of high photocatalysis activity, the optimal doping concentration of rare earth ions for the best UV luminescence property of upconversion material should be determined. Therefore, a range of different Yb^{3+} and Tm^{3+} doping concentration samples were prepared and tested with their upconversion luminescence intensity at 347 nm. The results are presented in Figure 2.4 and 2.5.

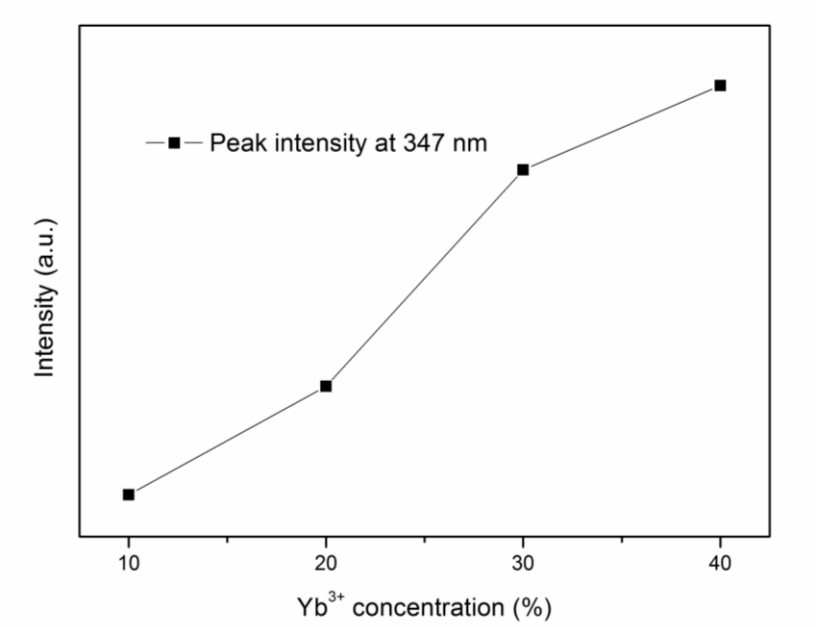

Figure 2.4 Influence of Yb concentration to the intensity of emission peak at 347 nm.

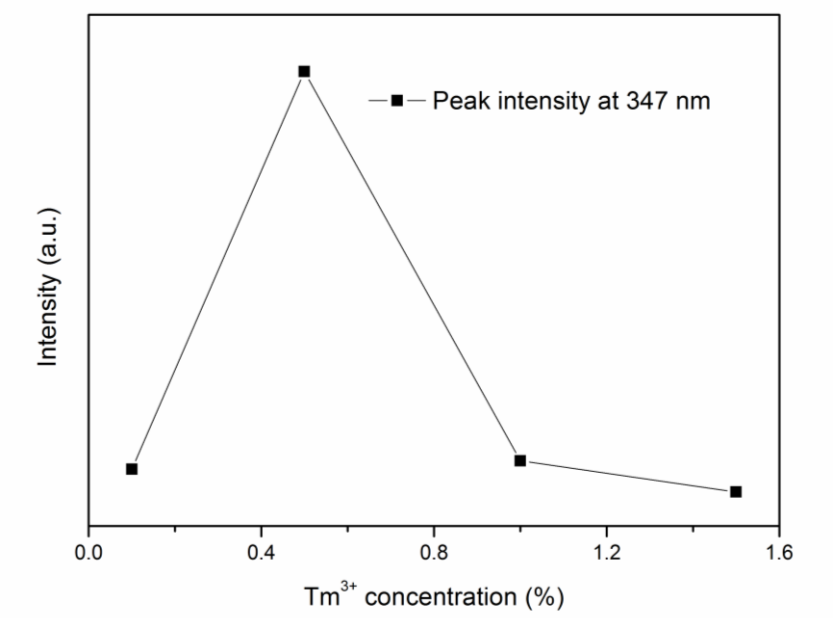

Figure 2.5 Influence of Tm concentration to the intensity of emission peak at 347 nm.

As mentioned above, Yb^{3+} ions acted as sensitizing agent in upconversion

luminescence process. Near-infrared laser energy can be absorbed by Yb^{3+} ions through $2F_{7/2}$ to $2F_{5/2}$ transition and transferred to Tm^{3+} ions to Yb^{3+} ions. As can be seen from Fig. 2.4, the intensity of emission peak at 347 nm increased as the Yb^{3+} doping concentration increased from 5% to 30%. This was due to higher possibility of Tm^{3+} transition to $^1D_6$ and $^1D_2$ orbit caused by higher Yb^{3+} ions.

At the same time, Tm^{3+} ions also played an important role as activating agent. Figure 2.5 presents upconversion emission intensity of samples with different Tm^{3+} doping concentration. When Yb^{3+} concentration was retained as 30%, the emission intensity increased first and then decreased with the increased Tm^{3+} concentration. The maximum emission intensity was obtained at 0.5% Tm^{3+} doping concentration. The subsequent decrease in emission intensity can be attributed to concentration quenching effect caused by excess Tm^{3+}.

Based on the above results, $NaYF_4$ with the strongest UV light emission can be obtained when the Tm^{3+} and Yb^{3+} doping concentrations were 0.5% and 30%. Therefore, $NaYF_4$: 30Yb, 0.5Tm was used as upconversion host in the subsequent synthesis and photocatalytic performance experiments.

This study adopted the EBS (emulsion-based bottom-up self-assembly) method [30] to assemble the 3D colloidal spheres. To test the validity of this

method, we first assembled the single nanocrystal ($NaYF_4$ or TiO_2, respectively). There were three main procedures in the assemble process: First, nanocrystals capped with ligands, well dispersed in cyclohexane were added to an aqueous solution of certain amount of SDS with a volume ratio of 1:10. Second, this system was microemulsified under magnetic stirring and ultrasonic treatment (oil droplets containing NCs are stabilized by SDS at the interface). Third, low-boiling solvent in the oil droplets was evaporated at a specified temperature under strong stirring, and the NCs in the confined oil droplet were assembled into 3D colloidal spheres, which can be well-dispersed in water. It was noteworthy that suitable conditions (nanocrystal concentration, surfactant concentration, stirring speed, and ultrasonic power) were essential to successful assemble. As shown in Table 2.1, regular and homogeneous 3D colloidal spheres could be obtained under ultrasonic cell crusher + Mechanical stirring at the same time rather than single ultrasonic cell crusher or mechanical stirring in emulsification process. NCs and SDS concentrations should be controlled at ~5 and ~10 mg/mL, respectively. Too low or too high concentration would result in irregular and inhomogeneous samples. The stirring speed at evaporation process could not be less than 1000 rpm. The suitable conditions for synthesis of 3D colloidal spheres are 5 mg/mL NCs concentration, 10 mg/mL SDS concentration, 1400 rpm stirring speed at

evaporation process with emulsification under ultrasonic cell crusher + Mechanical stirring.

Table 2.1 The morphology of 3D colloidal spheres and the experiment parameters

Emulsification process	NCs in oil phase (mg/mL)	SDS concentration (mg/mL)	Stirring speed at evaporation process (rpm)	Morphology of 3D colloidal spheres
Mechanical stirring	5	10	1400	Irregular shape, Inhomogeneous
Ultrasonic cell crusher	5	10	1400	Irregular shape, Inhomogeneous
Ultrasonic cell crusher+ Mechanical stirring	2.5 or 7.5	10	1400	Irregular shape, Inhomogeneous
Ultrasonic cell crusher+ Mechanical stirring	5	5 or 15	1400	Irregular shape, Inhomogeneous
Ultrasonic cell crusher+ Mechanical stirring	5	10	200-1000	Irregular shape, Inhomogeneous
Ultrasonic cell crusher+ Mechanical stirring	5	10	1400	regular shape, homogeneous

2.4.2 Characterization

The TEM images of original nanocrystal and the corresponding colloidal spheres are presented in Fig. 2.6. As can be seen, the size of $NaYF_4$ nanoparticles was ~22 nm, and it increased to hundreds of nanometers after assemble. Similarly, the size of TiO_2 nanoparticles and TiO_2 colloidal spheres was ~5 nm and ~100 nm, respectively. The TEM images demonstrated successful assemble of $NaYF_4$ or TiO_2. To test the upconversion emission property of $NaYF_4$ colloidal spheres, $NaYF_4$:Yb, Tm nanoparticles and $NaYF_4$: Yb, Tm colloidal spheres were dispersed in cyclohexane and irradiated by 980 nm diode continuous-wave (CW) laser. Figure 2.7 shows upconversion emission spectra of $NaYF_4$:Yb, Tm nanoparticles and $NaYF_4$:Yb, Tm colloidal spheres. There were five obvious peaks in the range of 250-500 nm: 290 nm, 347 nm, 362 nm, 452 nm, 476 nm, which were ascribed to $^1I_6 \rightarrow {}^2H_6$, $^1I_6 \rightarrow {}^2F_4$, $^1D_2 \rightarrow {}^3H_6$, $^1D_2 \rightarrow {}^3F_4$, $^1G_4 \rightarrow {}^3H_6$, respectively. The assemble would not change the upconversion emission property of upconversion materials since there was almost no change of the upconversion emission spectra after assemble.

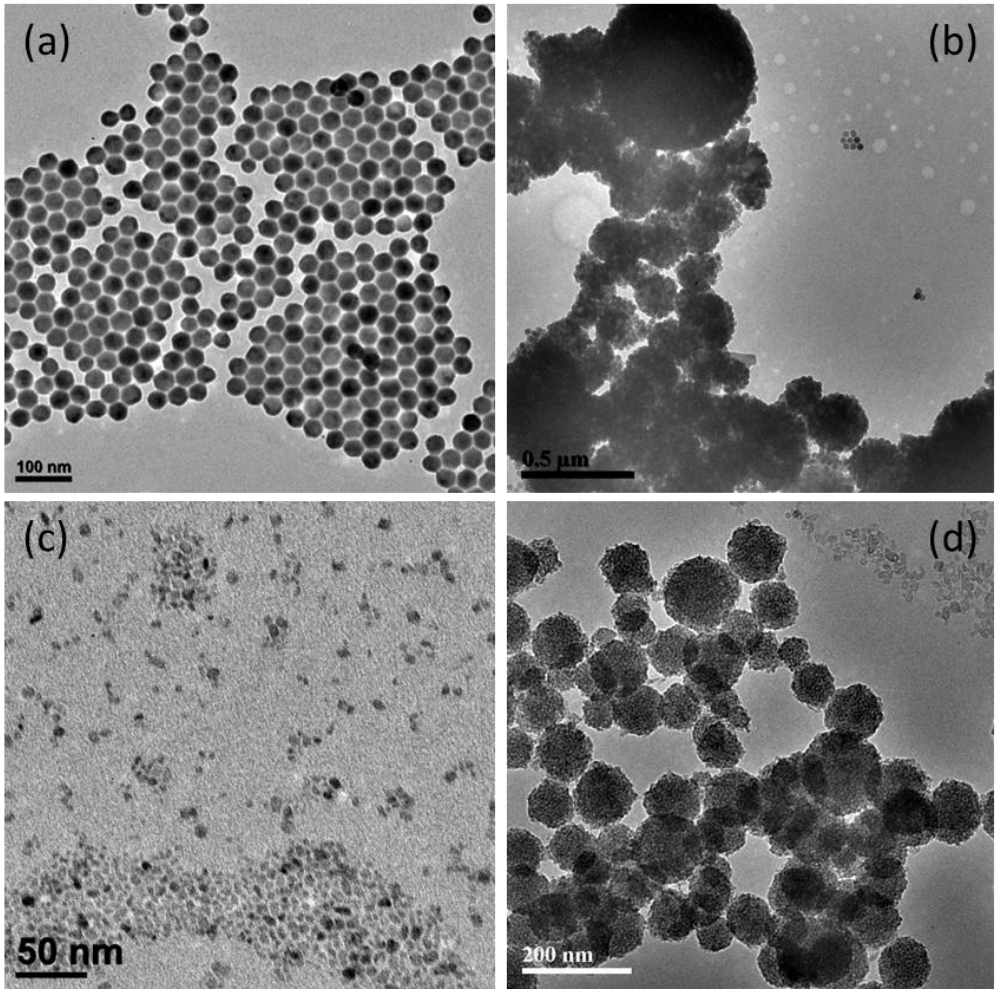

Figure 2.6 TEM images of (a) $NaYF_4$, (b) $NaYF_4$ colloidal spheres, (c) TiO_2, (d) TiO_2 colloidal shperes.

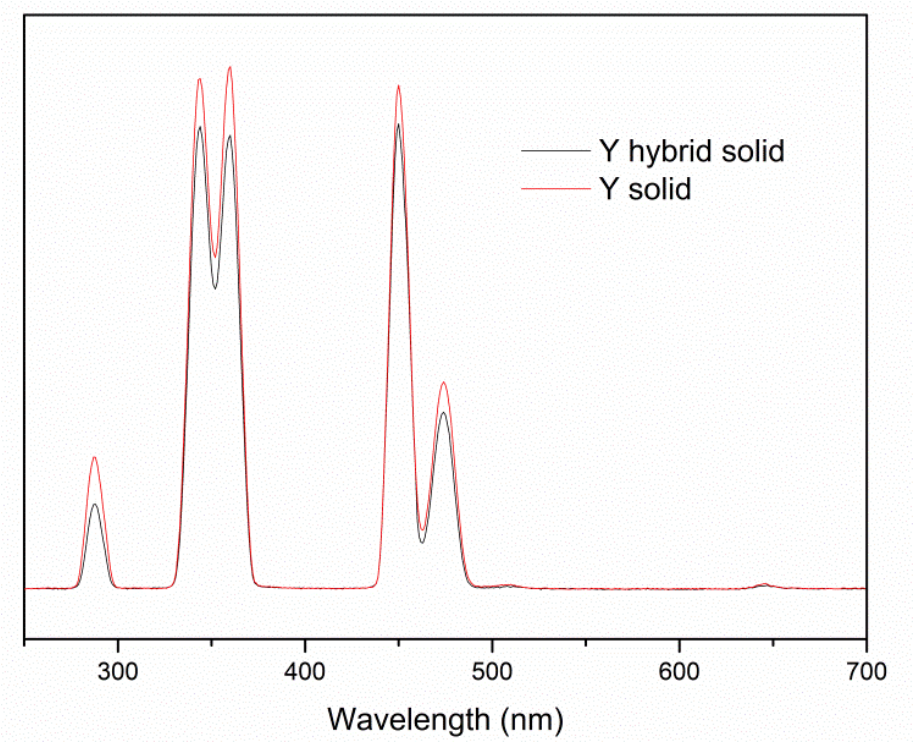

Figure 2.7 Upconversion emission spectra of $NaYF_4$:Yb, Tm nanoparticles (Y solid) and $NaYF_4$:Yb, Tm colloidal spheres (Y hybrid solid) in solid phase under excitation by a 980 nm continuous-wave (CW) laser.

The TEM and HRTEM images of $NaYF_4$: Yb, Tm-TiO_2 colloidal shperes are shown in Fig. 2.8 (inset: EDS spectra of $NaYF_4$: Yb, Tm-TiO_2 colloidal shperes). The diameter of $NaYF_4$: Yb, Tm-TiO_2 colloidal shperes was 200-400 nm. The EDS spectra indicated that there is Ti, Y, Yb elements in this colloidal shperes. It is worthwhile to note that Tm element couldn't be detected due to its low concentration. There were two different size nanoparticles in the HRTEM image. The size and the lattice distance of bigger one were ~22 nm and 0.2651 nm, respectively, which is ascribed to (200) plane of $NaYF_4$ nanocrystals. The size and the lattice distance of smaller one were ~5 nm and

0.3536 nm, respectively, which is ascribed to (101) plane of TiO2 nanocrystals. Moreover, the interparticle gap was about 1.8-2.2 nm, which is smaller than the double thickness of a contracted ligand monolayer (OA 1.7 nm). This phenomenon indicates the presence of chain interdigitation of the ligand layers among adjacent nanocrystals [30].

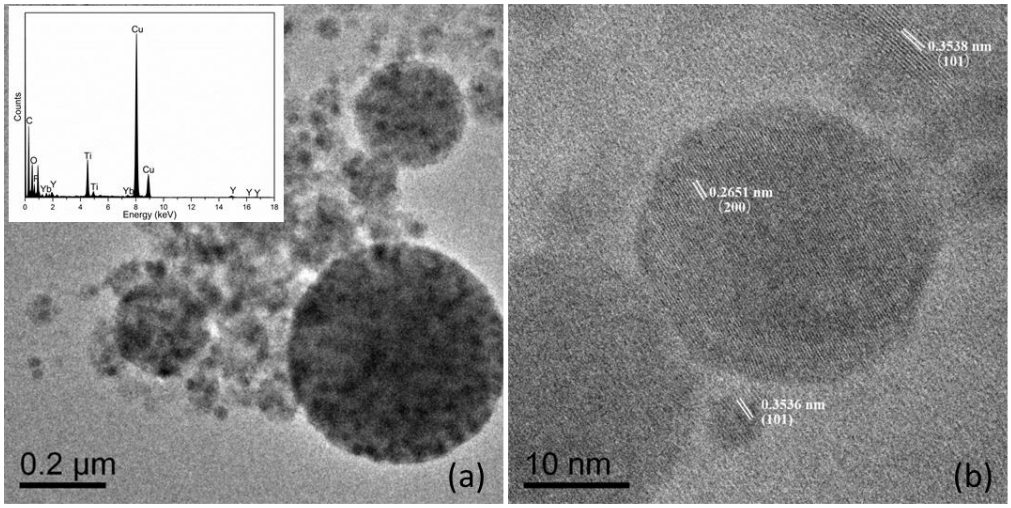

Figure 2.8 TEM image (a) of $NaYF_4$: Yb, Tm-TiO_2 colloidal shperes and HRTEM image (b) of aYF_4: Yb, Tm-TiO_2 colloidal shperes (inset: EDS spectra of $NaYF_4$: Yb, Tm-TiO_2 colloidal shperes).

XRD patterns of $NaYF_4$: Yb, Tm nanoparticles and $NaYF_4$: Yb, Tm-TiO_2 colloidal spheres are presented in Figure 2.9. As can be seen, apart from the typical peaks of $NaYF_4$, there are some new peaks (25.3^o, 37.8^o, 48.0^o, 55.1^o) in the XRD patterns of $NaYF_4$: Yb, Tm-TiO_2 colloidal spheres. These new peaks can be ascribed to (101), (004), (200), (211) planes of TiO_2 (JCPDs-21-1272). The sharp diffraction peaks of TiO2 demonstrated it had a

high degree of crystallinity.

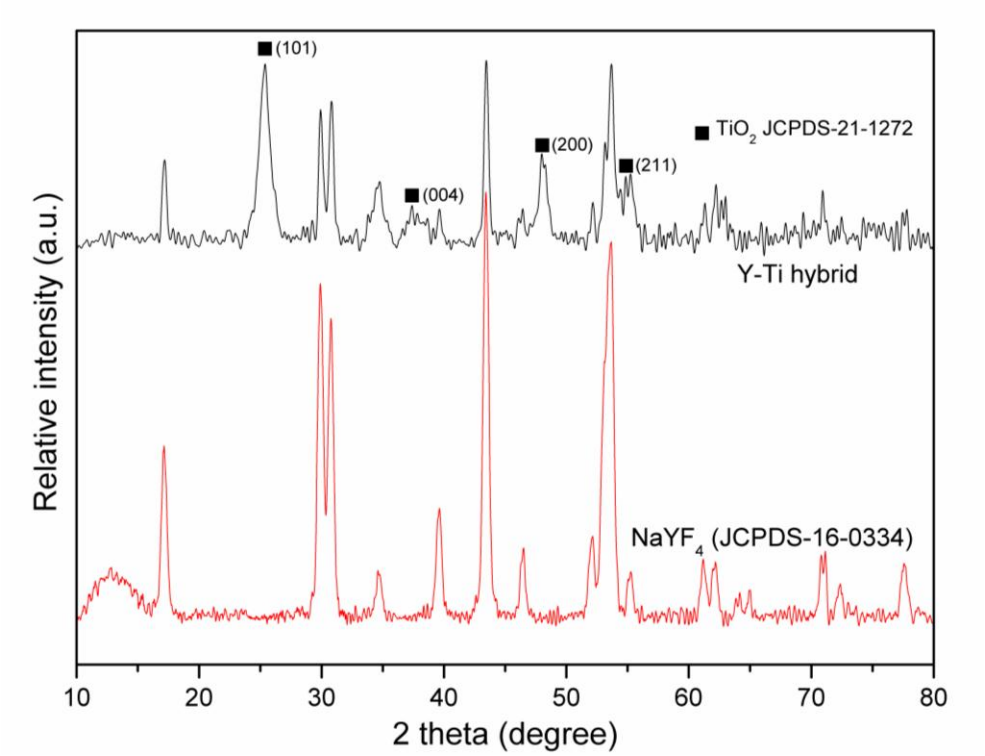

Figure 2.9 XRD patterns of $NaYF_4$: Yb, Tm nanoparticles and $NaYF_4$: Yb, Tm-TiO_2 colloidal spheres (Y-Ti hybrid).

2.4.3 The Upconversion Emission Property of $NaYF_4$:Yb,Tm-TiO_2 Colloidal Spheres

To test UV absorption property of $NaYF_4$:Yb,Tm-TiO_2 colloidal spheres, UV-vis absorption spectra of TiO_2, $NaYF_4$:Yb, Tm and $NaYF_4$:Yb, Tm-TiO_2 colloidal spheres were measured and presented in Fig. 2.10. $NaYF_4$:Yb, Tm showed almost no absorption throughout 200-1000 nm range. However, $NaYF_4$:Yb, Tm-TiO_2 colloidal spheres could absorb UV light with wavelength

less than 400 nm after assemble with TiO_2, which implied this material can make use of UV light for photocatalysis.

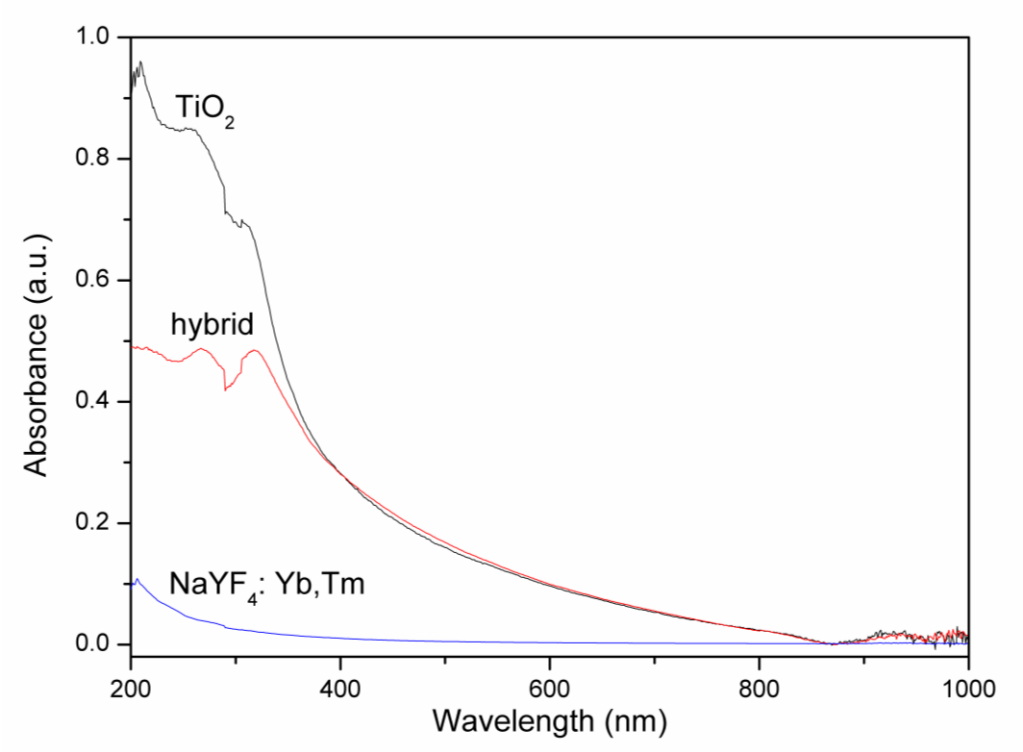

Figure 2.10 UV-vis absorption spectra of TiO_2, $NaYF_4$:Yb, Tm and $NaYF_4$:Yb, Tm-TiO_2 colloidal spheres (hybrid).

Figure 2.11 presents upconversion emission spectra of $NaYF_4$:Yb, Tm nanoparticles, $NaYF_4$:Yb, Tm-TiO_2 colloidal spheres, and mix material of $NaYF_4$:Yb, Tm and TiO_2 under excitation by a 980 nm continuous-wave (CW) laser. The five typical peaks in the range of 250-500 nm (290 nm, 347 nm, 362 nm, 452 nm, 476 nm) were ascribed to $^1I_6 \rightarrow {}^2H_6$, $^1I_6 \rightarrow {}^2F_4$, $^1D_2 \rightarrow {}^3H_6$, $^1D_2 \rightarrow {}^3F_4$,

$^1G_4 \rightarrow {}^3H_6$, respectively.

The three peaks of $NaYF_4$:Yb, Tm-TiO_2 colloidal spheres at UV region declined a lot compared to $NaYF_4$:Yb, Tm. The peak at 290 nm almost disappeared and the peak at 347 nm declined more than the peak at 362 nm. However, the peaks in the visible region showed almost no change.

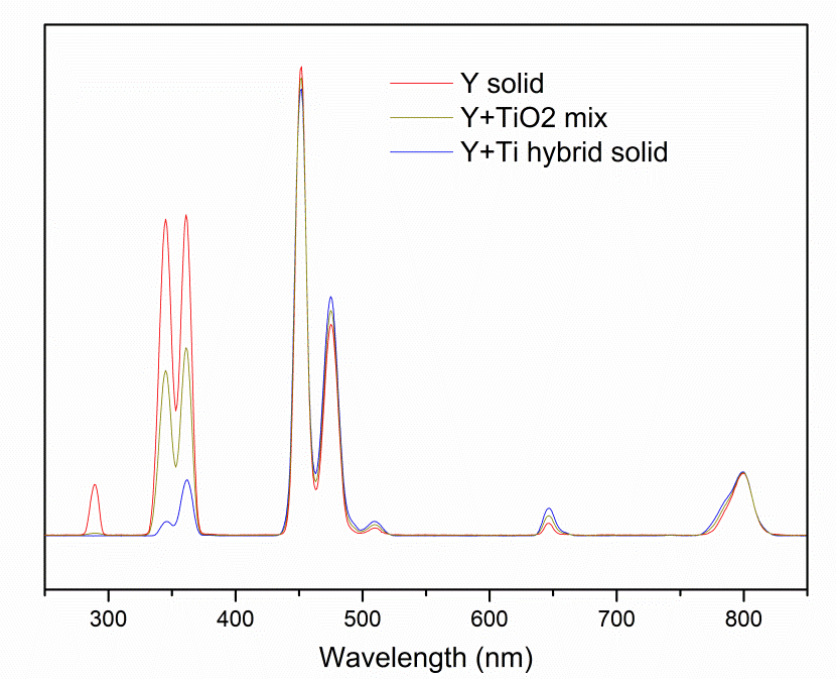

Figure 2.11 Upconversion emission spectra of $NaYF_4$:Yb, Tm nanoparticles (Y solid), $NaYF_4$:Yb, Tm+TiO_2 colloidal spheres (Y+Ti hybrid solid), and mix material of $NaYF_4$:Yb, Tm and TiO_2 (Y+TiO_2 mix) under excitation by a 980 nm continuous-wave (CW) laser.

To verify the high energy transfer efficiency of $NaYF_4$:Yb, Tm-TiO_2 colloidal spheres, the emission spectra of physical mixture of $NaYF_4$:Yb, Tm and TiO_2 was also measured. The emission intensity of physical mixture of

$NaYF_4$:Yb, Tm and TiO_2 at UV region was significantly higher than that of $NaYF_4$:Yb, Tm-TiO_2 colloidal spheres, which indicated that the latter one can fully utilized UV light emitted from upconversion materials.

2.4.4 NIR-responsive Photocatalytic Activity (980 nm) of $NaYF_4$: Yb, Tm-TiO_2 Colloidal Spheres

To achieve NIR-responsive photocatalysis, $NaYF_4$:Yb, Tm-TiO_2 colloidal spheres with a high degree of crystallinity had been prepared and it can fully utilized UV light emitted from upconversion materials. In this section, the photocatalytic properties of the samples under NIR excitation were tested and discussed.

The above experimental results showed that $NaYF_4$: Yb, Tm-TiO_2 colloidal spheres can effectively absorb UV light emitted from upconversion luminescence substrate. To confirm the absorption of ultraviolet light can excite TiO_2 to generate sufficient photo-generated electron-hole pairs to provide active radical substances required in the photocatalytic reaction, the following experiment was designed:

Terephthalic acid was used to capture photo-generated free radicals on TiO_2. The photo-generated holes located in the activated valence band of TiO_2 can react with water or hydroxyl to generate •OH for the degradation of organic pollutants. Terephthalic acid can react with •OH and generated one

fluorescent substance -- 2-hydroxy terephthalic acid, which can emit light at 425 nm under 320 nm excitation. Therefore, the detection of fluorescence emission peak of 2-hydroxy terephthalic acid can indicate generation of •OH. Specific reaction was as follows:

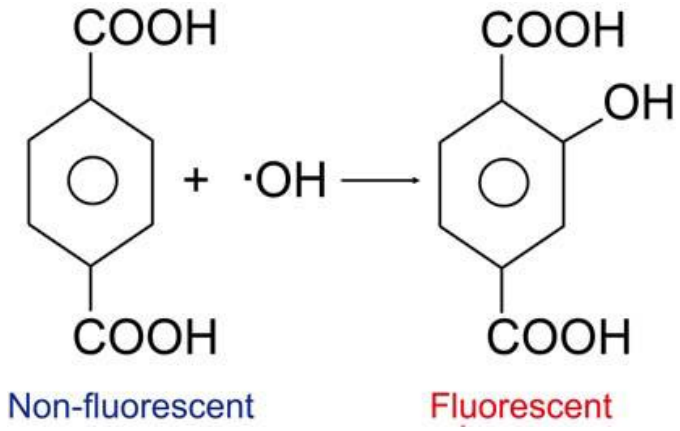

(2.1)

Time-dependent fluorescence spectra of the terephthalic acid solution under a 980 nm continuous-wave (CW) laser irradiation are presented in Fig. 2.12. As the irradiation time increased, the intensity of emission peak at 425 nm increased quickly. The results demonstrated that UV light energy emitted from upconversion materials had been utilized by TiO_2 to generate photo-generated electron-hole pairs, which then combined with the surface water or hydroxyl to generate sufficient amount of •OH for photocatalytic degradation of organic pollutants.

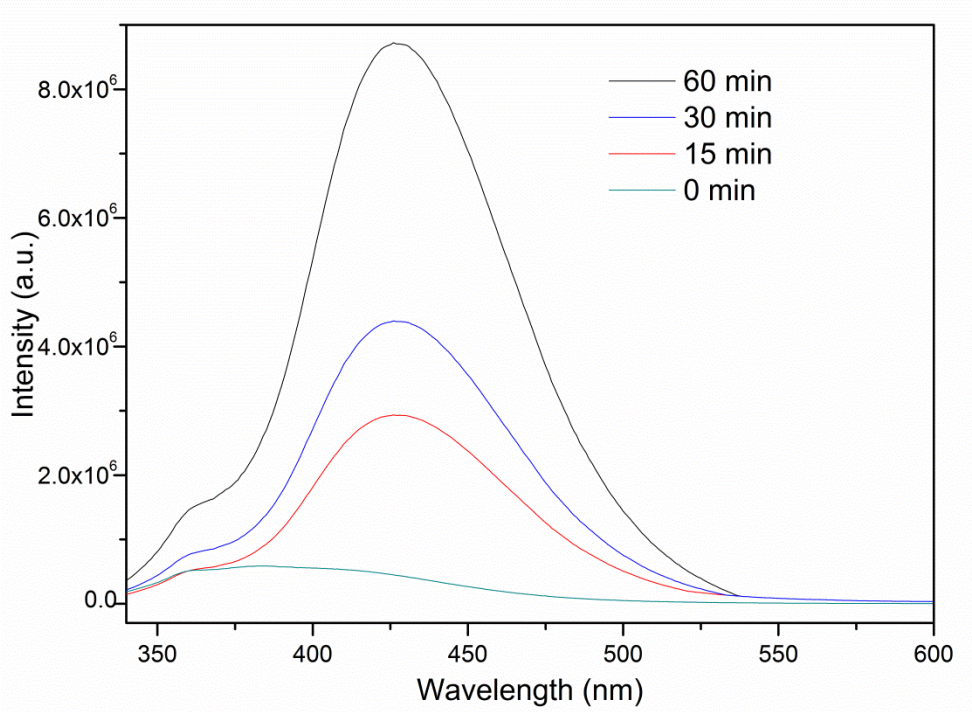

Figure 2.12 Time-dependent fluorescence spectra of the terephthalic acid solution under a 980 nm continuous-wave (CW) laser irradiation.

Four samples (NaYF4:Yb,Tm, TiO_2, mix material of $NaYF_4$:Yb, Tm and TiO_2, and NaYF4: Yb, Tm+TiO_2 colloidal spheres) were chosen for NIR photocatalytic activity experiments. The results are presented in Fig. 2.13. In the first two hours, the concentration of methylene blue in all samples increased. This anomaly was due to the heat caused by near-infrared laser irradiation. Temperature of the solution would increase because water molecules can absorb near-infrared light at certain wavelength. Therefore, a part of the MB dye molecules adsorbed on the surface of catalyst would desorb and enter into the liquid phase, resulting in the increase of MB

concentration. The temperature would reach equilibrium as the irradiation time further increased. So the differences in each sample gradually appeared after 2 h irradiation: TiO_2 and NaYF4: Yb, Tm did not exhibit significant catalytic activity (only 3% and 2% methylene blue was degraded after 8 h irradiation, respectively). The photocatalytic activity of mixture of $NaYF_4$:Yb, Tm and TiO_2 was much higher than the above two materials but still lower than NaYF4: Yb, Tm+TiO_2 colloidal spheres, which could be ascribed to the higher energy transfer efficiency of NaYF4: Yb, Tm+TiO_2 colloidal spheres than mix materials. After 8 h irradiation, 84% MB could be degraded by this new material.

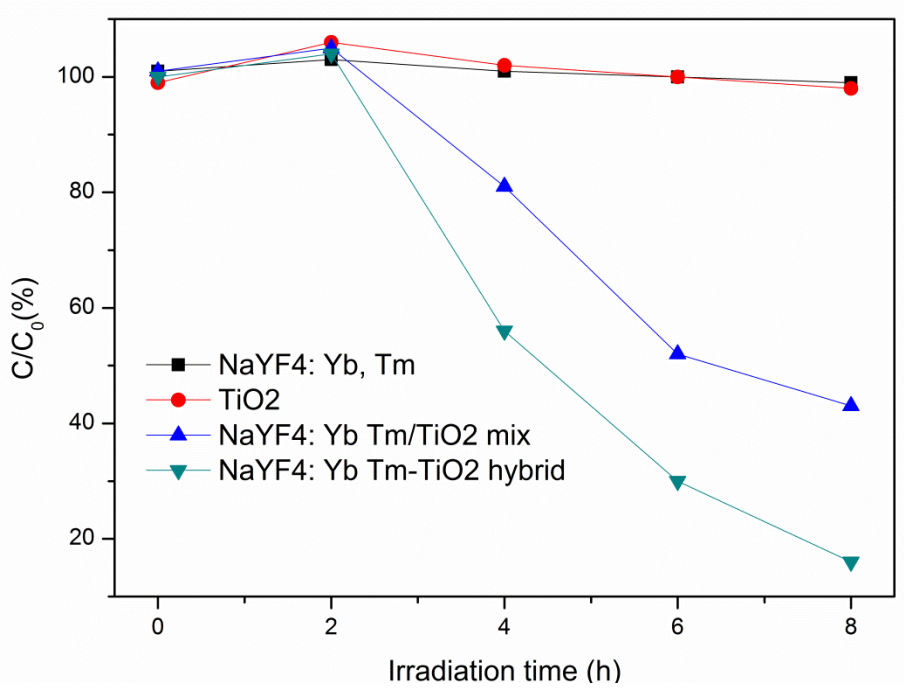

Figure 2.13 NIR photocatalytic activity of $NaYF_4$:Yb,Tm, TiO_2, mix material of $NaYF_4$:Yb, Tm and TiO_2, and NaYF4: Yb, Tm+TiO_2 colloidal spheres (980 nm). (2 g/L, 15 mg/L Methylene Blue)

2.5 Summary and Prospect

In conclusion, a new kind of photocatalyst (NaYF4: Yb, Tm+TiO_2 colloidal spheres) is successfully fabricated for NIR-responsive photocatalysis. The optimal synthesis conditions and doping concentration of rare earth ions for this new material are established. UV light energy emitted from upconversion materials has been utilized by this material to generate photo-generated electron-hole pairs, which then combine with the surface water or hydroxyl to generate sufficient amount of •OH for photocatalytic degradation of organic pollutants. This new material presents very good photocatalytic activity and could enhance utilization efficiency for solar energy.

CHAPTER 3: NIR-responsive Photocatalytic Activity (794 nm) $NaYF_4$:Yb, Tm, Nd@$NaYF_4$: Nd -TiO_2 Colloidal Spheres

3.1 Introduction

Rare earth doped materials have been widely investigated due to their unique advantages such as narrow emission band widths, large Stocks shift, long fluorescence lifetime, low biological toxicity and high physical and chemical stability [31]. Excitation wavelength near 980 nm, which matches the absorption by Yb^{3+} ions (commonly doped into nanoparticles as sensitizers), is always required. However, the absorption of Yb^{3+} ions largely overlap the absorption band of water molecules [32], which is unfavorable for the application of upconversion materials in water system because the 980 nm excitation source would be significantly attenuated when passing through water.

Recently, a lot of researchers have devoted to find suitable excitation wavelength to avoid the water absorption problem [32b, 33]. As can be seen from Fig. 3.1, this problem induced by 980 nm excitation could be largely alleviated using 800 nm laser excitation because of low absorption coefficients displayed by water molecules at 800 nm. The efficiency of NIR-responsive

photocatalytic activity would increase if the wavelength of response light for photocatalysis could be changed from 980 nm to 800 nm.

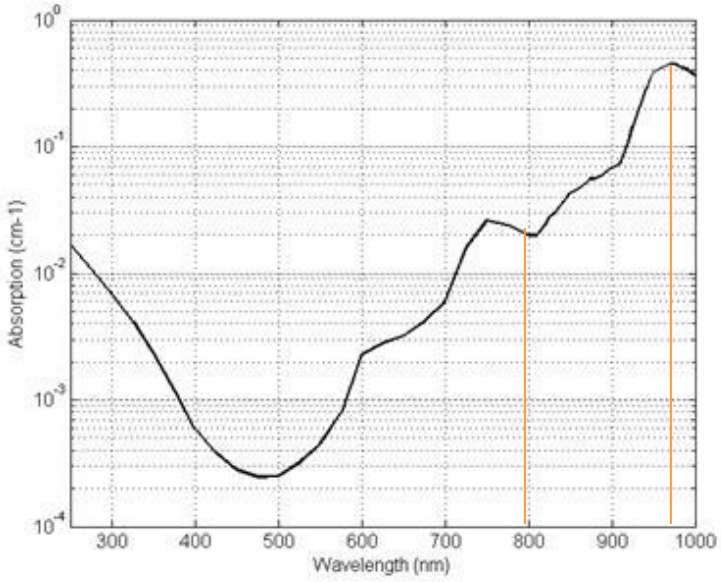

Figure 3.1 Water absorption spectra in vis-NIR region.

Nd^{3+}, which has a sharp absorption band around 800 nm, was doped as the sensitizer to achieve the photon upconversion under 800 nm [34]. However, Nd^{3+} can't reach very strong absorption at 800 nm and thus upconverted emission due to its low concentration doped in either bulk or nanoparticle systems [34]. The deleterious cross-relaxation between the Nd^{3+} and the activator ions would increase if doping a large amount of Nd^{3+} ions. Therefore, the intensity of upconversion emission of Nd^{3+}-based nanoparticles upon 800 nm irradiation is much lower than that of Yb^{3+}-based counterparts under 980 nm excitation.

Herein, we adopted Xie's design [9a] to increase the upconversion emission upon 800 nm excitation (Figure 3.2a). In this design, only 1-2 mol% of Nd^{3+} ions are doped into the core particle to avoid concentration quenching, while a relatively high concentration (~20 mol%) of Nd^{3+} ions are selectively doped within the shell layer for effectively harvesting light with wavelengths around 800 nm [35]. The absorption intensity at 794 nm of the nanoparticles with 20% Nd^{3+} doped in the shell layer is about 17 times higher than the controls without coating the Nd^{3+} shell layer (Figure 3.2b). This result indicates the feasibility of using Nd^{3+}-sensitized core-shell nanoparticles for NIR-responsive photocatalytic materials under 800 nm excitation.

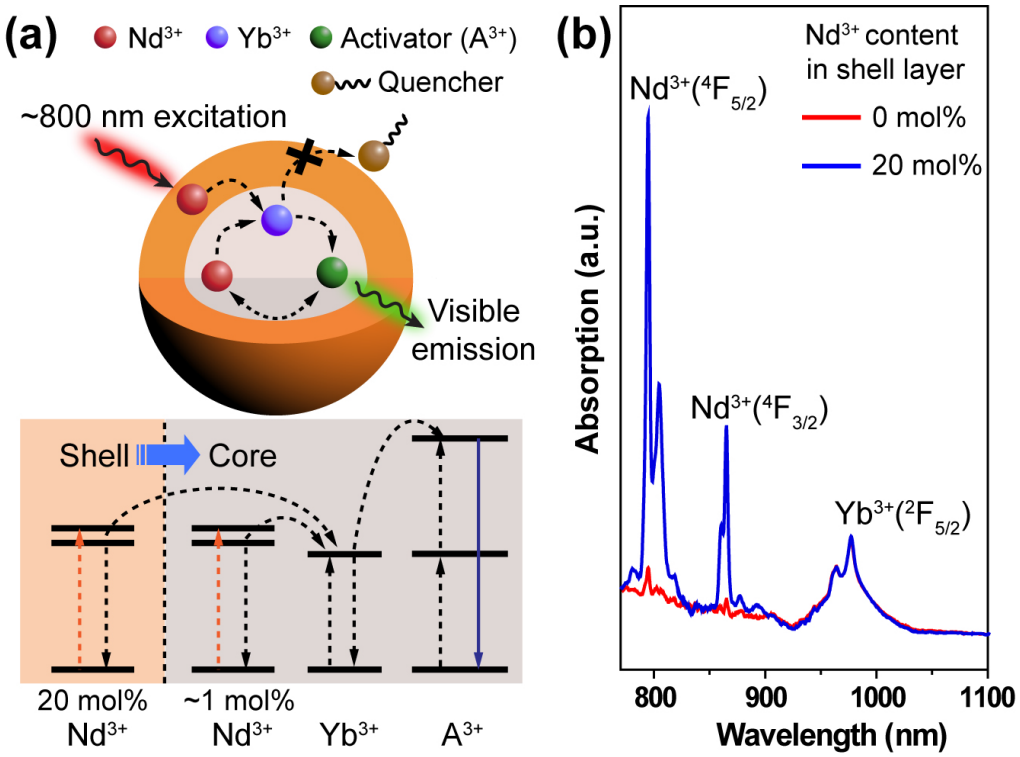

Figure 3.2 (a) Schematic design (top) and simplified energy level diagram

(bottom) of a core-shell nanoparticle for photon upconversion under 800 nm excitation. Nd^{3+} ions doped in the core and shell layers serve as sensitizers to absorb the excitation energy and subsequently transfer it to Yb^{3+} ions. After energy migration from the Yb^{3+} to activator ions, activator emission is achieved via the Nd^{3+}-sensitization process. (b) Near-infrared absorption spectra of the $NaYF_4$:Yb/Nd(30/1%) nanoparticles coated with an inert $NaYF_4$ shell and an active $NaYF_4$:Nd(20%) shell, respectively. Note that the absorption spectra were normalized at 976 nm for comparison. [36]

3.2 Synthesis and Characterization

3.2.1 Materials

Ammonium bicarbonate (NH_4HCO_3, 99.9%), triethylamine ($(C_2H_5)_3N$, >99%), titanium butoxide ($Ti(OCH_2CH_2CH_2CH_3)_4$, 97%), yttrium(III) acetate hydrate ($Y(CH_3CO_2)_3 \cdot xH_2O$, 99.9%), ytterbium(III) acetate hydrate($Yb(CH_3CO_2)_3 \cdot 4H_2O$, 99.9%), thulium acetate hydrate ($Tm(CH_3CO_2)_3 \cdot xH_2O$, 99.9%), neodymium(III) acetate hydrate ($Nd(CH_3CO_2)_3 \cdot xH_2O$, 99.9%), sodium hydroxide (NaOH, >98%), ammonium fluoride (NH_4F,>98%), 1-octadecene (90%), oleic acid (90%), cyclohexane (>99%), sodium dodecyl sulfate (SDS, >99%), methylene blue (MB, Fig. 2.2) were all purchased from Sigma-Aldrich and used as received unless otherwise noted. All other chemicals were purchased from Sigma-Aldrich unless otherwise noted.

3.2.2 Characterization

Low-resolution transmission electron microscopy (TEM) measurements were carried out on a JEOL-1400 transmission electron microscope (JEOL) operating at an acceleration voltage of 100 kV and high-resolution TEM measurements were carried out on a JEOL-JEM 2010F field emission transmission electron microscope operated at an acceleration voltage of 200 kV. Powder X-ray diffraction (XRD) data was recorded on a Siemens D5005 X-ray diffractometer with Cu Kα radiation (λ=1.5406 Å). The photoluminescence measurements were measured using a Spectra Physics Ti: sapphire oscillator (Tsunami) as the excitation source for ~800 nm excitation. UV-vis transmission spectrum was recorded on a SHIMADZU UV-3600 spectrophotometer. The CW laser beam was focused onto samples contained in a cuvette with path length of 1 cm. The emission from the samples was collected at an angle of 90^{o} to the excitation beam by a pair of lenses and an optical fiber that was connected to a monochromator (Acton, Spectra Pro 2300i) coupled CCD (Princeton Instruments, Pixis 100B). A short pass filter with a cutoff wavelength of 750 nm was placed before the monochromator to minimize scattering from the excitation beam. The upconversion luminescence spectra under 980 nm excitation were recorded in an Edinburgh FSP920 equipped with a photomultiplier (PMT), in conjunction with 980 nm diode laser (100 mW). The near-infrared photoluminescence spectrum was excited

by monochromatic light from a standard Xe lamp (450 W) passed through a monochromator (FSP920, Edinburgh).

3.2.3 Synthesis of $NaYF_4$: Yb^{3+}, Tm^{3+}, Nd^{3+} Nanoparticles

In a typical experiment [1], 2 mL water solution of $Ln(CH_3CO_2)_3$ (Ln = Y, Yb, Nd, 0.2 M, Ln = Tm, 0.02 M) was added to a 50-mL flask containing 3 mL of oleic acid. The mixture was heated at 150 ^oC for 30 min to remove water from the solution. Then 7 mL of 1-octadecene was quickly added to the flask and the resulting mixture was heated at 150 ^oC for another 30 min before cooling down to 50 ^oC. Shortly thereafter, 6 mL of methanol solution containing NH_4F (4 mL, 1.6 mmol) and NaOH (2 mL, 1 mmol) was added and the resultant solution was stirred for 30 min. The system temperature was heated to 100 ^oC to evaporated methanol and then argon was used to replace the air in this system. The solution was heated to 280 ^oC under argon for 1.5 h and then cooled down to room temperature. The resulting nanoparticles with a yield of 80 mg were precipitated by addition of ethanol, collected by centrifugation at 6000 rpm for 5 min, washed with ethanol several times, and re-dispersed in 4 mL of cyclohexane.

3.2.4 Synthesis of $NaYF_4$:Yb/Tm/Nd@$NaYF_4$:Nd Core-Shell Nanoparticles

A water solution (2 mL) of $Y(CH_3CO_2)_3$ and $Nd(CH_3CO_2)_3$ was added into a 50-mL flask containing oleic acid (3 mL). The mixture was heated at 150 ^oC for 30 min to remove water from the solution. Then 7 mL of 1-octadecene was quickly added to the flask and the resulting mixture was heated at 150 ^oC for another 30 min before cooling down to 50 ^oC. As-synthesized $NaYF_4$:Yb/Tm/Nd nanoparticles in 4 mL of cyclohexane were added along with a 6 mL methanol solution containing NH_4F (4 mL, 1.6 mmol) and NaOH (2 mL, 1 mmol). The resulting mixture was stirred at 50 ^oC for 30 min, at which time the reaction temperature was increased to 100 ^oC to remove the methanol. Then the solution was heated to 290 ^oC under an argon flow for 1.5 h and then cooled to room temperature. The resulting nanoparticles were precipitated out by the addition of ethanol, collected by centrifugation, washed with ethanol, and redispersed in cyclohexane.

3.2.5 Synthesis of Titanium Dioxide Nanoparticles

In the typical synthesis procedure of TiO_2 nanoparticles [29], 0.5 g NH_4HCO_3, 7 mL OA, and 3 mL triethylamine were mixed at room temperature by magnetic stirring. Then $Ti(OBu)_4$ (1 mL) was added dropwise into the solution. After continued stirring at room temperature for 5 min, the solution was transferred into a Teflon-lined, stainless autoclave at 150 ^oC for

24 h. TiO_2 nanoparticles were obtained.

3.2.6 Synthesis of $NaYF_4$:Yb/Tm/Nd@$NaYF_4$:Nd -TiO_2 Hybrid

In a general preparation of water-dispersed 3D colloidal spheres from oil-dispersed NCs [30], SDS (200 mg) was added to deionized water (20 mL). A solution containing upconversion materials (0.5 mL) and TiO_2 (1.5 mL) in cyclohexane was added to the aqueous solution. This system was then emulsified by ultrasonic treatment together with magnetic stirring. The cyclohexane was removed by heating at 70 ^oC with constant stirring for 4 h to assemble the NCs into 3D spheres. After the reaction was cooled to room temperature, the products were collected and purified by repeated centrifugation and were redispersed. The final products were stored in water.

3.3 Photocatalytic Experiments

Photocatalysis was performed via monitoring methyl blue (MB) degradation by measuring the optical absorption using a Shimadzu UV-3600 spectrophotometer. In a typical experiment, 4 mg of the $NaYF_4$:Yb/Tm/Nd@$NaYF_4$:Nd -TiO_2 hybrid was dispersed into a quartz cuvette containing 2 mL of MB aqueous solution (15 mg L^{-1}) and then kept in the dark prior to irradiation for reaching adsorption−desorption equilibrium of

MB on the surface of materials before irradiation. A laser of 794 nm with a power of 2 W was used as the irradiation source. After irradiation of 794 nm light for a designated time, 0.3 mL of the MB aqueous solution was taken out and centrifuged for UV−vis absorbance measurements. The concentration of MB solution at each time interval was calculated using the calibration curve of the characteristic absorption peak of MB (663 nm) of the standard solution.

3.4 Results and Discussion

3.4.1 Characterization

The TEM images of $NaYF_4$:Yb/Tm/Nd nanocrystal and $NaYF_4$:Yb/Tm/Nd@$NaYF_4$:Nd core-shell nanoparticles are presented in Fig. 3.3. As can be seen, the size of $NaYF_4$:Yb/Tm/Nd nanoparticles was ~22 nm, and that of $NaYF_4$:Yb/Tm/Nd@$NaYF_4$:Nd nanoparticles increased to ~25 nm due to the coating with a shell of $NaYF_4$:Nd. The shape of $NaYF_4$:Yb/Tm/Nd@$NaYF_4$:Nd nanoparticles was more irregular than $NaYF_4$:Yb/Tm/Nd, which confirmed the core-shell structure.

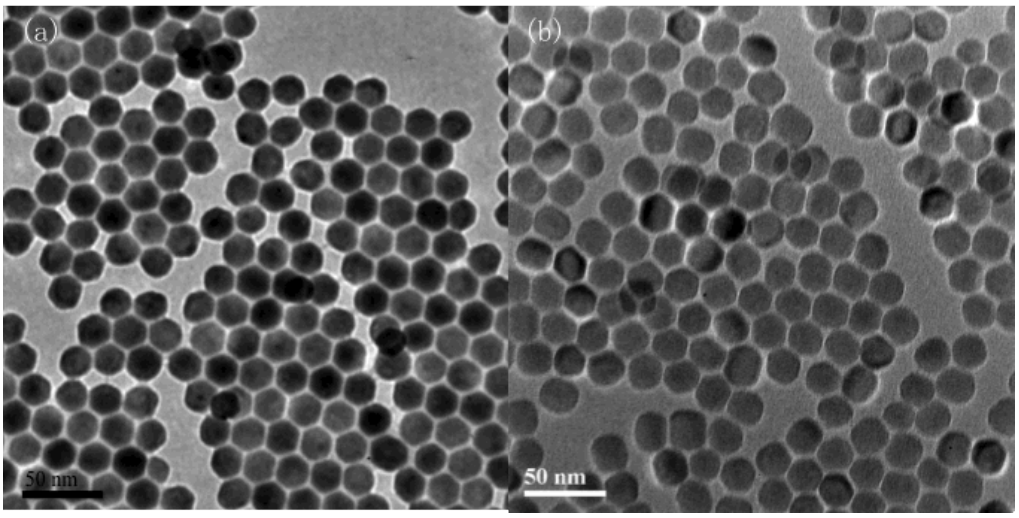

Figure 3.3 TEM images of (a) $NaYF_4$:Yb/Tm/Nd, (b) $NaYF_4$:Yb/Tm/Nd@$NaYF_4$:Nd.

XRD patterns of $NaYF_4$:Yb/Tm/Nd nanoparticles and $NaYF_4$:Yb/Tm/Nd@$NaYF_4$:Nd-TiO_2 colloidal spheres are presented in Figure 3.4. As can be seen, apart from the typical peaks of hexagonal $NaYF_4$, there are some new peaks (25.3^o, 37.8^o, 48.0^o) in the XRD patterns of $NaYF_4$:Yb, Tm, Nd@$NaYF_4$: Nd-TiO_2 colloidal spheres. These new peaks can be ascribed to (101), (004), (200) planes of TiO_2 (JCPDs-21-1272). The sharp diffraction peaks of TiO2 demonstrated it had a high degree of crystallinity.

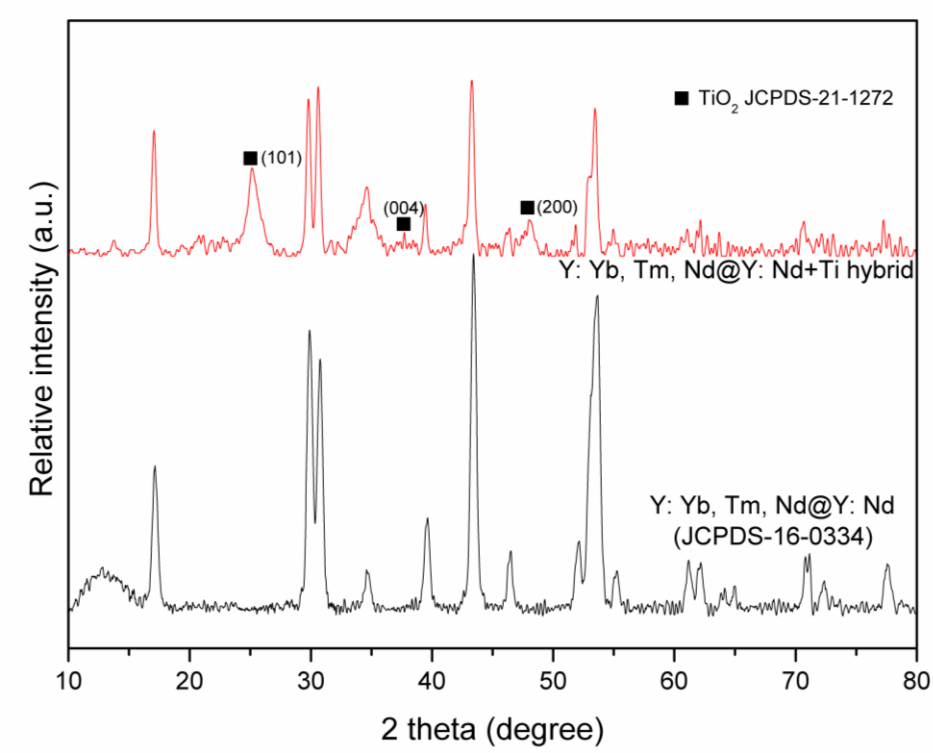

Figure 3.4 XRD patterns of $NaYF_4$ and $NaYF_4$:Yb, Tm, Nd@$NaYF_4$: Nd-TiO_2 colloidal spheres (hybrid).

Figure 3.5 shows the proposed energy transfer mechanism in $NaYF_4$ nanoparticles doped with Yb/Tm/Nd under 794 nm CW laser excitation. The Nd^{3+} ions, whcih act as sensitizers, sensitize the activators (Tm^{3+}). However, the energy was not directly transferred to Tm^{3+} from Nd^{3+}. The Yb^{3+} ions serve as migrators to transfer the energy of Nd^{3+} to activators. The energy transfer between Nd^{3+} ($^4F_{3/2}$) and Yb^{3+} ($^2F_{5/2}$) was so efficient that the whole energy transfer efficiency was comparable to that of $NaYF_4$:Yb, Tm under 980 nm excitation [9a].

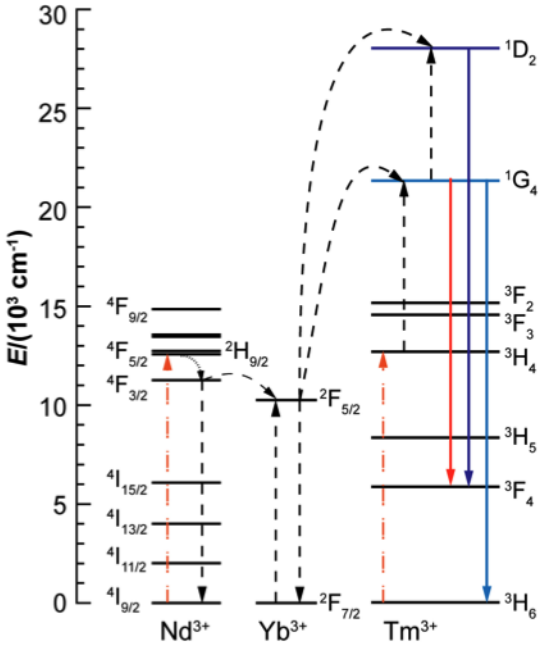

Figure 3.5 Proposed energy transfer mechanisms under 794 nm CW laser excitation in $NaYF_4$ nanoparticles doped with Yb/Tm/Nd. The dashed-dotted, dashed, dotted, and full arrows represent photon excitation, energy transfer, multiphonon relaxation, andemission process, respectively. For clarity, only dominated energy transfer processes are shown in the proposed mechanisms.[36]

3.4.2 The Upconversion Emission Property of $NaYF_4$:Yb, Tm, Nd@$NaYF_4$: Nd-TiO_2 colloidal spheres

According to the above energy transfer mechanism, $NaYF_4$:Yb, Tm, Nd@$NaYF_4$: Nd was supposed to be excited by both 980 nm and 794 nm. To verify this assumption, upconversion emission spectra of $NaYF_4$:Yb, Tm, Nd@$NaYF_4$: Nd under 980 nm excitation (2 W), 794 nm excitation (2 W), and 980 nm+794 nm excitation (2 W+2 W) were measured (Figure 3.6). It should be noted that the sample was irradiated by both 980 nm and 794 nm laser at the same time. It can be seen that there was upconversion emission under

either 980 nm or 794 nm excitation. More importantly, the intensity of upconversion emission under 980 nm+794 nm excitation was stronger than under either 980 nm or 794 nm excitation. It can be inferred that $NaYF_4$:Yb, Tm, Nd@$NaYF_4$: Nd can not only utilized 794 nm light but also 980 nm light when irradiated by solar light.

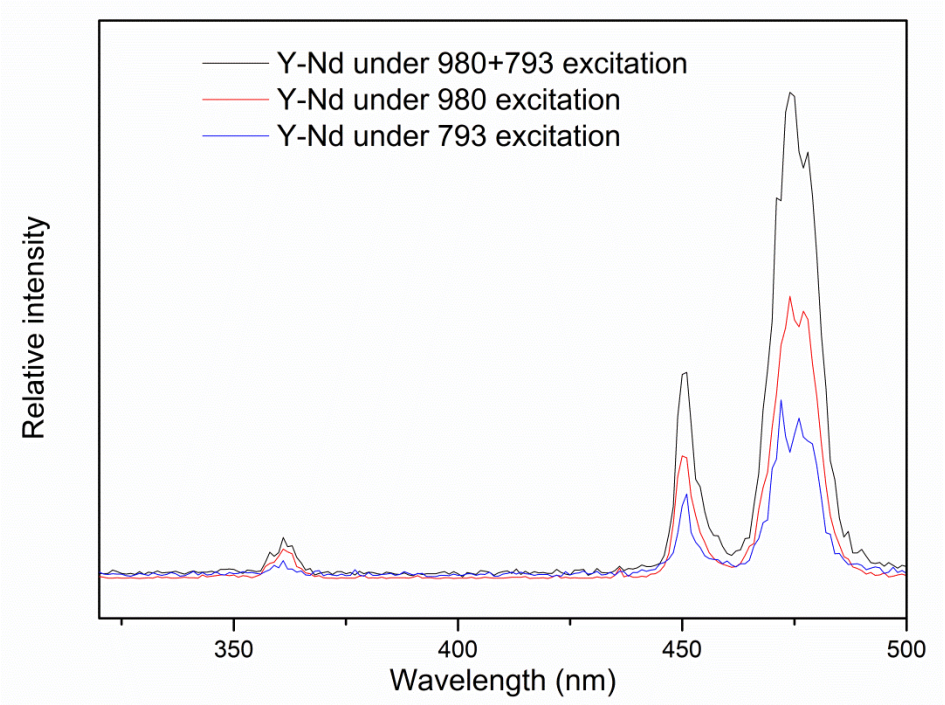

Figure 3.6 Upconversion emission spectra of $NaYF_4$:Yb, Tm, Nd@$NaYF_4$: Nd under 980 nm excitation, 794 nm excitation, and 980 nm+794 nm excitation.

Upconversion emission spectra of $NaYF_4$:Yb, Tm, Nd@$NaYF_4$: Nd (Y-Nd solid) and $NaYF_4$:Yb, Tm, Nd@$NaYF_4$: Nd-TiO_2 colloidal spheres (Y-Nd+Ti solid) under excitation by a 980 nm continuous-wave (CW) laser are presented in Fig. 3.7. The four typical peaks in the range of 300-500 nm (347 nm, 362

nm, 452 nm, 476 nm) were ascribed to $^1I_6 \rightarrow {}^2F_4$, $^1D_2 \rightarrow {}^3H_6$, $^1D_2 \rightarrow {}^3F_4$, $^1G_4 \rightarrow {}^3H_6$, respectively.

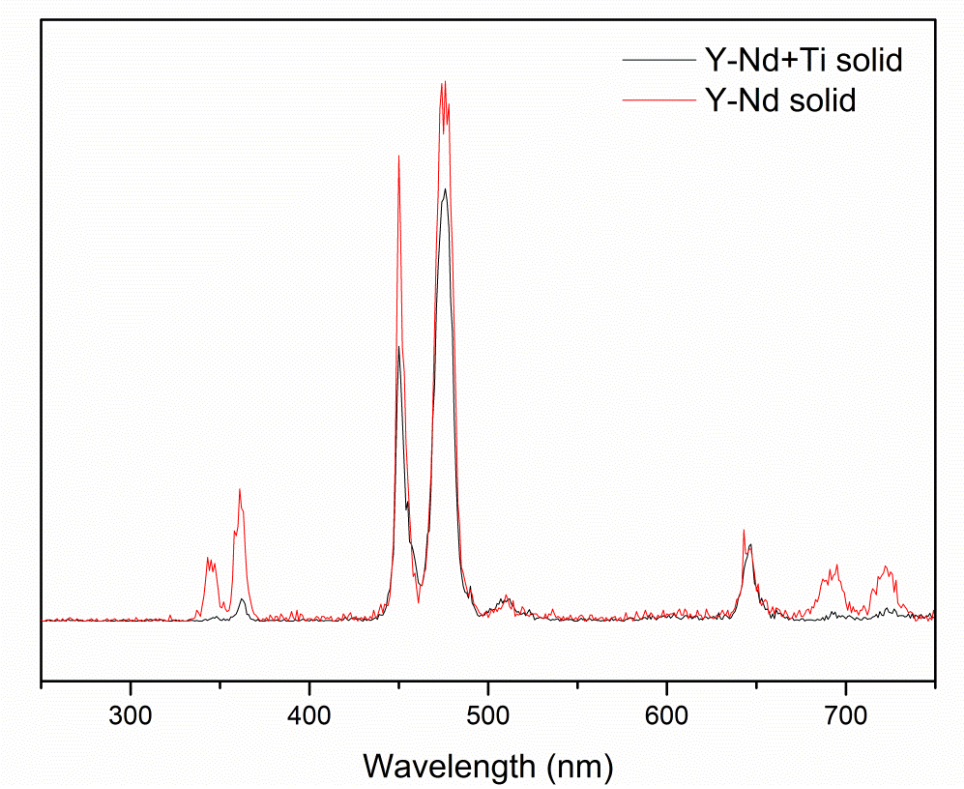

Figure 3.7 Upconversion emission spectra of $NaYF_4$:Yb, Tm, Nd@$NaYF_4$: Nd (Y-Nd solid) and $NaYF_4$:Yb, Tm, Nd@$NaYF_4$: Nd-TiO_2 colloidal spheres (Y-Nd+Ti solid) under excitation by a 980 nm continuous-wave (CW) laser.

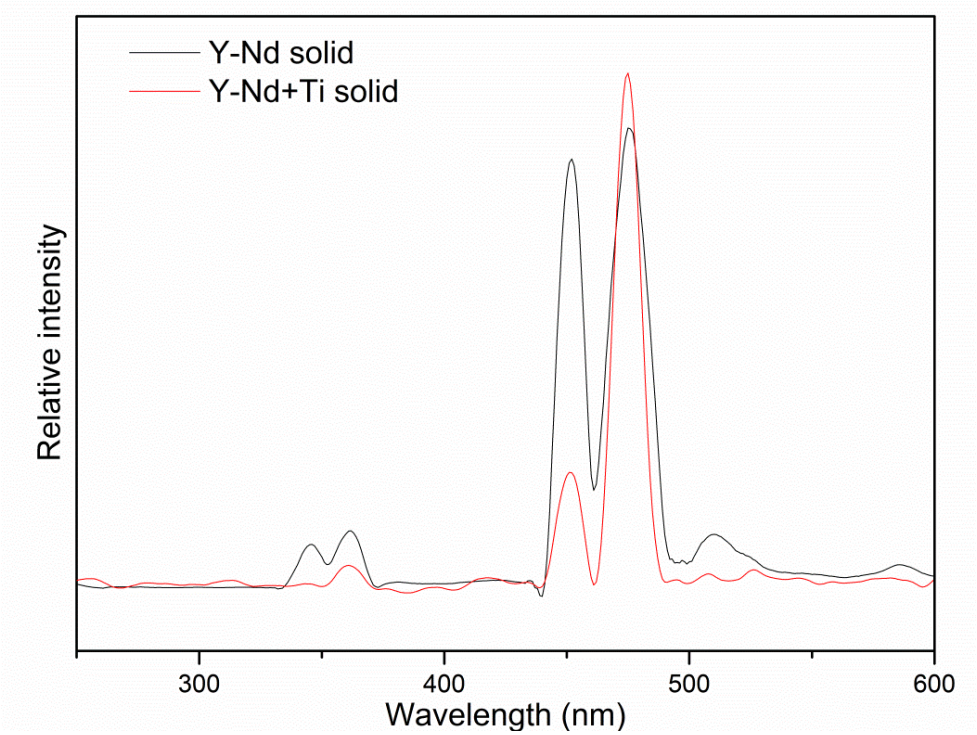

Figure 3.8 Upconversion emission spectra of $NaYF_4$:Yb, Tm, Nd@$NaYF_4$: Nd (Y-Nd solid) and $NaYF_4$:Yb, Tm, Nd@$NaYF_4$: Nd-TiO_2 hybrid (Y-Nd+Ti solid) under 794 nm excitation.

Compared with the two peaks of $NaYF_4$:Yb, Tm, Nd@$NaYF_4$: Nd at UV region, that of $NaYF_4$:Yb, Tm, Nd@$NaYF_4$: Nd-TiO_2 hybrid declined a lot. However, the peaks at 400-500 nm region showed almost no change. This result should be due to the UV absorption property of TiO_2. The similar experimental phenomena could be observed when excited by 794 nm laser (Figure 3.8).

3.4.3 NIR-responsive Photocatalytic Activity (794 nm) of $NaYF_4$: Yb, Tm-TiO_2 Colloidal Spheres

To achieve NIR-responsive photocatalysis under 794 nm excitation, $NaYF_4$:Yb, Tm, Nd@$NaYF_4$: Nd-TiO_2 colloidal spheres had been prepared. The above experimental results showed that this material could effectively absorb UV light emitted from upconversion nanoparticles.

Four samples ($NaYF_4$:Yb/Tm,/Nd@$NaYF_4$:Nd, TiO_2, mix material of $NaYF_4$:Yb/Tm/Nd@$NaYF_4$:Nd and TiO_2, and $NaYF_4$:Yb/Tm/Nd@$NaYF_4$: Nd-TiO_2 colloidal spheres) were chosen for NIR photocatalytic activity experiments (Fig. 3.9). Unlike NIR photocatalytic activity experiment in the chapter 2, the concentration of methylene blue in all samples decreased in the first two hours, which confirmed that there was no heating effect caused by water absorption of irradiation light. Therefore, there was almost no energy consumption by water and consequent heating effect. TiO_2 and $NaYF_4$:Yb/Tm,/Nd@$NaYF_4$:Nd did not exhibit significant catalytic activity. The photocatalytic activity of mixture of $NaYF_4$:Yb/Tm/Nd@$NaYF_4$:Nd and TiO_2 was much higher than the above two materials but still lower than $NaYF_4$:Yb/Tm/Nd@$NaYF_4$: Nd-TiO_2 colloidal spheres, which could degraded 85% MB after 8 h irradiation.

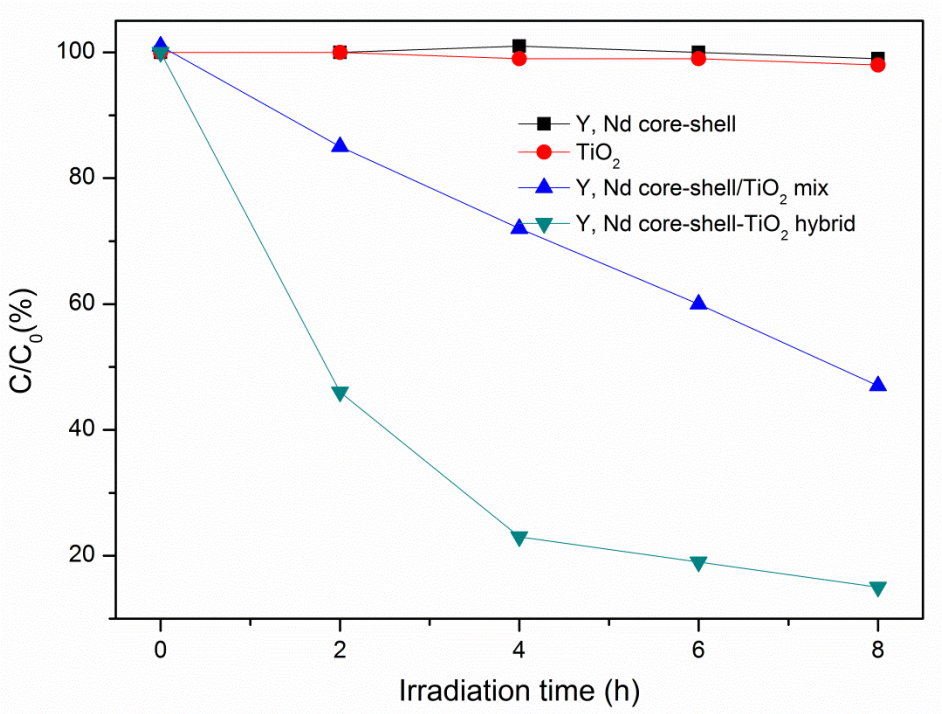

Figure 3.9 NIR photocatalytic activity of $NaYF_4$:Yb/Tm,/Nd@$NaYF_4$:Nd, TiO_2, mix material of $NaYF_4$:Yb/Tm/Nd@$NaYF_4$:Nd and TiO_2, and $NaYF_4$:Yb/Tm/Nd@$NaYF_4$: Nd-TiO_2 colloidal spheres (794 nm).

3.5 Summary and Prospect

In conclusion, the new kind of photocatalyst ($NaYF_4$:Yb/Tm/Nd@$NaYF_4$:Nd-TiO_2 colloidal spheres) is successfully fabricated and it showed high energy transfer efficiency. $NaYF_4$:Yb/Tm/Nd@$NaYF_4$:Nd-TiO_2 colloidal spheres can not only utilize 794 nm light but also 980 nm light when irradiated by solar light. Besides, this new material can avoid energy consumption by water and consequent heating effect under 980 nm excitation. 85% MB can be degraded by

$NaYF_4$:Yb/Tm/Nd@$NaYF_4$:Nd-TiO_2 colloidal spheres, which confirms it good potential for photcatalytic application.

CHAPTER 4: Conclusions and Future Work

The primary purpose of this study was to extend excitation source of photocatalysis of typical photocatalyst (TiO_2). Two new kind of photocatalyst (NaYF4:Yb, Tm-TiO_2 and $NaYF_4$:Yb, Tm, Nd@$NaYF_4$: Nd-TiO_2 colloidal spheres) were successfully fabricated for NIR-responsive photocatalysis. This design enhanced the active surface area and thus the photocatalytic efficiency compared to the core-shell structure. The main conclusions are as follows:

Firstly, the 3D colloidal spheres are designed and the optimal synthesis conditions for them are 5 mg/mL NCs concentration, 10 mg/mL SDS concentration, 1400 rpm stirring speed at evaporation process with emulsification under ultrasonic cell crusher + Mechanical stirring. $NaYF_4$ with the strongest UV light emission can be obtained when the Tm^{3+} and Yb^{3+} doping concentrations were 0.5% and 30%. UV light energy emitted from upconversion materials has been utilized by this material to generate photo-generated electron-hole pairs, which then combine with the surface water or hydroxyl to generate sufficient amount of •OH for photocatalytic degradation of organic pollutants. This new material presents very good photocatalytic activity and could enhance utilization efficiency for solar

energy.

Secondly, $NaYF_4$:Yb/Tm/Nd@$NaYF_4$:Nd-TiO_2 colloidal spheres is successfully fabricated and it showed high energy transfer efficiency. This new material can not only utilize 794 nm light but also 980 nm light when irradiated by solar light. Besides, it can avoid energy consumption by water and consequent heating effect under 980 nm excitation. 85% MB can be degraded by $NaYF_4$:Yb/Tm/Nd@$NaYF_4$:Nd-TiO_2 colloidal spheres, which confirms its good potential for photcatalytic application.

The results of this present study may have significant impact on the photocatalysis of organic pollutant under different NIR light excitation. The newly designed structure could make full use of the total surface area of $NaYF_4$: Yb^{3+}, Tm^{3+} and TiO_2 nanoparticles. Moreover, the NIR responsive photocatalysis under 794 nm excitation could offer a new direction for the utilization of solar light with different wavelength.

Considering the research in the intergration of photolysts and upconversion nanoparticles is still at an infant stage, there are several interesting directions for future work in the areas of research presented in this thesis.

The light source used in this study corresponds to the absorption wavelength of Yb^{3+} and Nd^{3+} ions. However, making full use of sunlight needs

extension of certain near infrared light and more expansion region. Therefore, more sensitizers should be employed to extend utilization of solar light. Secondly, the existing shell of pure phase anatase TiO_2 nanocrystals can be further modified, which could be doping or secondary composite heterostructure, to further enhance its light conversion efficiency.

References

1. Wang, F.; Deng, R.; Wang, J.; Wang, Q.; Han, Y.; Zhu, H.; Chen, X.; Liu, X., Tuning upconversion through energy migration in core–shell nanoparticles. *Nature Materials* **2011,** *10* (12), 968-973.

2. (a) Chen, C.; Ma, W.; Zhao, J., Semiconductor-mediated photodegradation of pollutants under visible-light irradiation. *Chemical Society Reviews* **2010,** *39* (11), 4206-4219; (b) Froschl, T.; Hormann, U.; Kubiak, P.; Kucerova, G.; Pfanzelt, M.; Weiss, C. K.; Behm, R. J.; Husing, N.; Kaiser, U.; Landfester, K.; Wohlfahrt-Mehrens, M., High surface area crystalline titanium dioxide: potential and limits in electrochemical energy storage and catalysis. *Chemical Society Reviews* **2012,** *41* (15), 5313-5360; (c) Chen, X.; Shen, S.; Guo, L.; Mao, S. S., Semiconductor-based Photocatalytic Hydrogen Generation. *Chemical Reviews* **2010,** *110* (11), 6503-6570.

3. Li, Y.-F.; Chen, C., Fate and Toxicity of Metallic and Metal-Containing Nanoparticles for Biomedical Applications. *Small* **2011,** *7* (21), 2965-2980.

4. Auzel, F., Upconversion and anti-stokes processes with f and d ions in solids. *Chemical Reviews* **2004,** *104* (1), 139-173.

5. Wang, F.; Liu, X., Recent advances in the chemistry of lanthanide-doped upconversion nanocrystals. *Chemical Society Reviews* **2009,** *38* (4), 976-989.

6. (a) Akira Fujishima; Honda, K., Electrochemical Photolysis of Water at a Semiconductor Electrode. *Nature* **1972,** *238*, 37-38; (b) Fujishima, A.; Zhang, X.; Tryk, D. A., TiO2 photocatalysis and related surface phenomena. *Surface Science Reports* **2008,** *63* (12), 515-582.

7. Wang, F.; Banerjee, D.; Liu, Y.; Chen, X.; Liu, X., Upconversion nanoparticles in biological labeling, imaging, and therapy. *Analyst* **2010,** *135* (8), 1839-1854.

8. Huang, X.; Han, S.; Huang, W.; Liu, X., Enhancing solar cell efficiency: the search for luminescent materials as spectral converters. *Chemical Society Reviews* **2013,** *42* (1), 173-201.

9. (a) Xie, X.; Gao, N.; Deng, R.; Sun, Q.; Xu, Q.-H.; Liu, X., Mechanistic Investigation of Photon Upconversion in Nd3+-Sensitized Core–Shell Nanoparticles. *Journal of the American Chemical Society* **2013,** *135* (34), 12608-12611; (b) Wang, Y.-F.; Liu, G.-Y.; Sun, L.-D.; Xiao, J.-W.; Zhou, J.-C.; Yan, C.-H., Nd3+-Sensitized Upconversion Nanophosphors: Efficient In Vivo Bioimaging Probes with Minimized Heating Effect. *Acs Nano* **2013,** *7* (8), 7200-7206.

10. Haase, M.; Schaefer, H., Upconverting Nanoparticles. *Angewandte Chemie-International Edition* **2011,** *50* (26), 5808-5829.

11. Su, Q.; Han, S.; Xie, X.; Zhu, H.; Chen, H.; Chen, C.-K.; Liu, R.-S.; Chen,

X.; Wang, F.; Liu, X., The Effect of Surface Coating on Energy Migration-Mediated Upconversion. *Journal of the American Chemical Society* **2012,** *134* (51), 20849-20857.

12. (a) de Wild, J.; Meijerink, A.; Rath, J. K.; van Sark, W. G. J. H. M.; Schropp, R. E. I., Upconverter solar cells: materials and applications. *Energy & Environmental Science* **2011,** *4* (12), 4835; (b) Fischer, S.; Goldschmidt, J. C.; Loeper, P.; Bauer, G. H.; Brueggemann, R.; Kraemer, K.; Biner, D.; Hermle, M.; Glunz, S. W., Enhancement of silicon solar cell efficiency by upconversion: Optical and electrical characterization. *Journal of Applied Physics* **2010,** *108* (4).

13. (a) Hoffmann, M. R.; Martin, S. T.; Choi, W. Y.; Bahnemann, D. W., ENVIRONMENTAL APPLICATIONS OF SEMICONDUCTOR PHOTOCATALYSIS. *Chemical Reviews* **1995,** *95* (1), 69-96; (b) Kabra, K.; Chaudhary, R.; Sawhney, R. L., Treatment of hazardous organic and inorganic compounds through aqueous-phase photocatalysis: A review. *Industrial & Engineering Chemistry Research* **2004,** *43* (24), 7683-7696.

14. Daghrir, R.; Drogui, P.; Robert, D., Modified TiO2 For Environmental Photocatalytic Applications: A Review. *Industrial & Engineering Chemistry Research* **2013,** *52* (10), 3581-3599.

15. Chen, X.; Liu, L.; Yu, P. Y.; Mao, S. S., Increasing Solar Absorption for

Photocatalysis with Black Hydrogenated Titanium Dioxide Nanocrystals. *Science* **2011,** *331* (6018), 746-750.

16. Li, Z.-X.; Shi, F.-B.; Zhang, T.; Wu, H.-S.; Sun, L.-D.; Yan, C.-H., Ytterbium stabilized ordered mesoporous titania for near-infrared photocatalysis. *Chemical Communications* **2011,** *47* (28), 8109-8111.

17. Qin, W.; Zhang, D.; Zhao, D.; Wang, L.; Zheng, K., Near-infrared photocatalysis based on YF3 : Yb3+, Tm3+/TiO2 core/shell nanoparticles. *Chemical Communications* **2010,** *46* (13), 2304-2306.

18. (a) Zhang, Y.; Hong, Z., Synthesis of lanthanide-doped NaYF4@TiO2 core–shell composites with highly crystalline and tunable TiO2 shells under mild conditions and their upconversion-based photocatalysis. *Nanoscale* **2013,** *5* (19), 8930; (b) Tang, Y.; Di, W.; Zhai, X.; Yang, R.; Qin, W., NIR-Responsive Photocatalytic Activity and Mechanism of NaYF4:Yb,Tm@TiO2Core–Shell Nanoparticles. *ACS Catalysis* **2013,** *3* (3), 405-412; (c) Wang, W.; Ding, M.; Lu, C.; Ni, Y.; Xu, Z., A study on upconversion UV–vis–NIR responsive photocatalytic activity and mechanisms of hexagonal phase NaYF4:Yb3+,Tm3+@TiO2 core–shell structured photocatalyst. *Applied Catalysis B: Environmental* **2014,** *144*, 379-385.

19. Maira, A. J.; Yeung, K. L.; Lee, C. Y.; Yue, P. L.; Chan, C. K., Size effects in gas-phase photo-oxidation of trichloroethylene using nanometer-sized TiO2

catalysts. *Journal of Catalysis* **2000,** *192* (1), 185-196.

20. Lue, Q.; Guo, F.; Sun, L.; Li, A.; Zhao, L., Silica-/titania-coated Y(2)O(3): Tm(3+),Yb(3+) nanoparticles with improvement in upconversion luminescence induced by different thickness shells. *Journal of Applied Physics* **2008,** *103* (12).

21. (a) Wang, W.; Lu, C.-H.; Ni, Y.-R.; Song, J.-B.; Su, M.-X.; Xu, Z.-Z., Enhanced visible-light photoactivity of {001} facets dominated TiO2 nanosheets with even distributed bulk oxygen vacancy and Ti3+. *Catalysis Communications* **2012,** *22*, 19-23; (b) Wang, W.; Lu, C.; Ni, Y.; Su, M.; Huang, W.; Xu, Z., Preparation and characterization of visible-light-driven N–F–Ta tri-doped TiO2 photocatalysts. *Applied Surface Science* **2012,** *258* (22), 8696-8703; (c) Lee, J. S.; You, K. H.; Park, C. B., Highly Photoactive, Low Bandgap TiO2 Nanoparticles Wrapped by Graphene. *Advanced Materials* **2012,** *24* (8), 1084-1088; (d) Yu, J.; Ma, T.; Liu, S., Enhanced photocatalytic activity of mesoporous TiO2 aggregates by embedding carbon nanotubes as electron-transfer channel. *Physical Chemistry Chemical Physics* **2011,** *13* (8), 3491-3501; (e) Zhu, H.; Yang, B.; Xu, J.; Fu, Z.; Wen, M.; Guo, T.; Fu, S.; Zuo, J.; Zhang, S., Construction of Z-scheme type CdS–Au–TiO2 hollow nanorod arrays with enhanced photocatalytic activity. *Applied Catalysis B: Environmental* **2009,** *90* (3–4), 463-469; (f) An, W.-J.; Wang, W.-N.;

Ramalingam, B.; Mukherjee, S.; Daubayev, B.; Gangopadhyay, S.; Biswas, P., Enhanced Water Photolysis with Pt Metal Nanoparticles on Single Crystal TiO2 Surfaces. *Langmuir* **2012,** *28* (19), 7528-7534.

22. D'Arienzo, M.; Siedl, N.; Sternig, A.; Scotti, R.; Morazzoni, F.; Bernardi, J.; Diwald, O., Solar Light and Dopant-Induced Recombination Effects: Photoactive Nitrogen in TiO2 as a Case Study. *The Journal of Physical Chemistry C* **2010,** *114* (42), 18067-18072.

23. Ren, L.; Qi, X.; Liu, Y.; Huang, Z.; Wei, X.; Li, J.; Yang, L.; Zhong, J., Upconversion-P25-graphene composite as an advanced sunlight driven photocatalytic hybrid material. *Journal of Materials Chemistry* **2012,** *22* (23), 11765-11771.

24. Xu, Q. C.; Zhang, Y.; Tan, M. J.; Liu, Y.; Yuan, S.; Choong, C.; Tan, N. S.; Tan, T. T. Y., Anti-cAngptl4 Ab-Conjugated N-TiO2/NaYF4:Yb,Tm Nanocomposite for Near Infrared-Triggered Drug Release and Enhanced Targeted Cancer Cell Ablation. *Advanced Healthcare Materials* **2012,** *1* (4), 470-474.

25. Wang, F.; Wang, J.; Liu, X., Direct Evidence of a Surface Quenching Effect on Size-Dependent Luminescence of Upconversion Nanoparticles. *Angewandte Chemie-International Edition* **2010,** *49* (41), 7456-7460.

26. Li, C.; Wang, F.; Zhu, J.; Yu, J. C., NaYF4 Yb,Tm/CdS composite as a

novel near-infrared-driven photocatalyst. *Applied Catalysis B-Environmental* **2010,** *100* (3-4), 433-439.

27. Li, X., Multifunctional Upconversion-Magnetic Hybrid Nanostructured Materials: Synthesis and Bioapplications. *Theranostics* **2013,** *3* (5), 292-305.

28. Huang, S.; Gu, L.; Miao, C.; Lou, Z.; Zhu, N.; Yuan, H.; Shan, A., Near-infrared photocatalyst of Er3+/Yb3+ codoped (CaF2@TiO2) nanoparticles with active-core/active-shell structure. *Journal of Materials Chemistry A* **2013,** *1* (27), 7874-7879.

29. Li, X.-L.; Peng, Q.; Yi, J.-X.; Wang, X.; Li, Y., Near Monodisperse TiO2 Nanoparticles and Nanorods. *Chemistry - A European Journal* **2006,** *12* (8), 2383-2391.

30. Bai, F.; Wang, D.; Huo, Z.; Chen, W.; Liu, L.; Liang, X.; Chen, C.; Wang, X.; Peng, Q.; Li, Y., A Versatile Bottom-up Assembly Approach to Colloidal Spheres from Nanocrystals. *Angewandte Chemie International Edition* **2007,** *46* (35), 6650-6653.

31. (a) Deng, R.; Xie, X.; Vendrell, M.; Chang, Y.-T.; Liu, X., Intracellular Glutathione Detection Using MnO2-Nanosheet-Modified Upconversion Nanoparticles. *Journal of the American Chemical Society* **2011,** *133* (50), 20168-20171; (b) Zhang, F.; Shi, Q.; Zhang, Y.; Shi, Y.; Ding, K.; Zhao, D.; Stucky, G. D., Fluorescence Upconversion Microbarcodes for Multiplexed

Biological Detection: Nucleic Acid Encoding. *Advanced Materials* **2011,** *23* (33), 3775-+; (c) Teng, X.; Zhu, Y.; Wei, W.; Wang, S.; Huang, J.; Naccache, R.; Hu, W.; Tok, A. I. Y.; Han, Y.; Zhang, Q.; Fan, Q.; Huang, W.; Capobianco, J. A.; Huang, L., Lanthanide-Doped NaxScF3+x Nanocrystals: Crystal Structure Evolution and Multicolor Tuning. *Journal of the American Chemical Society* **2012,** *134* (20), 8340-8343.

32. (a) Zhan, Q.; Qian, J.; Liang, H.; Somesfalean, G.; Wang, D.; He, S.; Zhang, Z.; Andersson-Engels, S., Using 915 nm Laser Excited Tm3+/Er3+/Ho3+-Doped NaYbF4 Upconversion Nanoparticles for in Vitro and Deeper in Vivo Bioimaging without Overheating Irradiation. *Acs Nano* **2011,** *5* (5), 3744-3757; (b) Zou, W.; Visser, C.; Maduro, J. A.; Pshenichnikov, M. S.; Hummelen, J. C., Broadband dye-sensitized upconversion of near-infrared light. *Nature Photonics* **2012,** *6* (8), 560-564.

33. Zhan, Q.; He, S.; Qian, J.; Cheng, H.; Cai, F., Optimization of Optical Excitation of Upconversion Nanoparticles for Rapid Microscopy and Deeper Tissue Imaging with Higher Quantum Yield. *Theranostics* **2013,** *3* (5), 306-316.

34. (a) Lin, H.; Chen, D.; Yu, Y.; Shan, Z.; Huang, P.; Wang, Y.; Yuan, J., Nd3+-sensitized upconversion white light emission of Tm3+/Ho3+ bridged by Yb3+ in beta-YF3 nanocrystals embedded transparent glass ceramics. *Journal*

of Applied Physics **2010,** *107* (10); (b) Zhou, J.; Shirahata, N.; Sun, H.-T.; Ghosh, B.; Ogawara, M.; Teng, Y.; Zhou, S.; Chu, R. G. S.; Fujii, M.; Qiu, J., Efficient Dual-Modal NIR-to-NIR Emission of Rare Earth Ions Co-doped Nanocrystals for Biological Fluorescence Imaging. *Journal of Physical Chemistry Letters* **2013,** *4* (3), 402-408.

35. (a) Vetrone, F.; Naccache, R.; Mahalingam, V.; Morgan, C. G.; Capobianco, J. A., The Active-Core/Active-Shell Approach: A Strategy to Enhance the Upconversion Luminescence in Lanthanide-Doped Nanoparticles. *Advanced Functional Materials* **2009,** *19* (18), 2924-2929; (b) Yang, D.; Li, C.; Li, G.; Shang, M.; Kang, X.; Lin, J., Colloidal synthesis and remarkable enhancement of the upconversion luminescence of BaGdF5:Yb3+/Er3+ nanoparticles by active-shell modification. *Journal of Materials Chemistry* **2011,** *21* (16), 5923-5927.

36. Xie, X.; Gao, N.; Deng, R.; Sun, Q.; Xu, Q.-H.; Liu, X., Mechanistic Investigation of Photon Upconversion in Nd3+-Sensitized Core-Shell Nanoparticles. *Journal of the American Chemical Society* **2013,** *135* (34), 12608-12611.